Comprehensive evaluation of typical planetary boundary layer (PBL) parameterization schemes in China. Part II: Influence of uncertainty factors

Wenxing Jia[1], Xiaoye Zhang[1,2*], Hong Wang[1], Yaqiang Wang[1], Deying Wang[1], Junting Zhong[1], Wenjie Zhang[1], Lei Zhang[1], Lifeng Guo[1], Yadong Lei[1], Jizhi Wang[1], Yuanqin Yang[1], Yi Lin[3]

[1]State Key Laboratory of Severe Weather & Key Laboratory of Atmospheric Chemistry of CMA, Chinese Academy of Meteorological Sciences, Beijing, 100081, China

[2]Center for Excellence in Regional Atmospheric Environment, IUE, Chinese Academy of Sciences, Xiamen, 361021, China

[3]Key Laboratory for Mesoscale Severe Weather, Ministry of Education, and School of Atmospheric Sciences, Nanjing University, Nanjing, 210023, China

Correspondence to: X. Zhang (xiaoye@cma.gov.cn)

31   **Abstract.** This study focuses on the uncertainties that influence numerical simulation results of

32   meteorological fields (including horizontal resolution: 75 km, 15km and 3 km, vertical resolution:

33   48 and 62 levels, near-surface (N-S) scheme: MM5 and Eta schemes, initial and boundary conditions:

34   Final (FNL) and European Center for Medium-Range Weather Forecasting (ECMWF) reanalysis

35   data, underlying surface update: model default and latest updates, and update of model version:

36   version 3.6.1 and 3.9.1). By further evaluating and analyzing the uncertainty factors, it is expected

37   to provide relevance for those scholars who are devoted to factor analysis, in order to make the

38   results closer to the observed values. In this study, a total of 12 experiments are set up to analyze

39   the effects of the uncertainties mentioned above, and the following conclusions are drawn: (1)

40   Horizontal resolution has a greater effect than vertical resolution. (2) The simulated effects of

41   temperature and wind speed in the N-S scheme are smaller than those in the PBL scheme. (3) The

42   initial and boundary conditions of different products have the most remarkable effect on relative

43   humidity, and the simulation results of ECMWF data are the best. (4) The updates with urban and

44   water bodies as the underlying surface have a more significant contribution to the meteorological

45   fields, especially on temperature. (5) For the PBL parameterization schemes, the update of the model

46   version has less impact on the simulation results, because each update has small changes and no

47   major changes overall. In general, the configuration of uncertainties needs to be considered

48   comprehensively according to what you need in order to obtain the best simulation results.

49

50   **Introduction**

51   The key factor for the accurate simulation of near-surface (N-S) meteorological parameters and

52   planetary boundary layer (PBL) structures is the PBL parameterization scheme. Part I has discussed

53   the impact of the PBL schemes in detail from the mechanism, and assessed the applicability of the

54   PBL schemes for different parameters (i.e., 2-m temperature, 2-m relative humidity, 10-m wind

55   speed and direction, PBL vertical structures, PBL height, turbulent diffusion coefficient) in different

56   regions (i.e., North China Plain, NCP; Yangtze River Delta, YRD; Sichuan Basin, SB; Pearl River

57   Delta, PRD and Northwest Semi-arid, NS) and seasons (i.e., January, April, July and October).

58   However, there are still many uncertainties in the model that can affect the forecasts and model

59   results. The model settings used by different scholars exhibit differences in the simulation results.

60   For example, the horizontal and vertical resolutions are essential for model settings. Horizontal

resolution, as a critical factor, must be considered in all models, whether they are macroscale earth system models (Ma-ESMs), climate models (CMs) mesoscale weather models (Me-WMs), or microscale fluid models (Mi-FMs). Constrained by computational resources, a horizontal resolution of about 100~250 km is used for Ma-ESMs models (e.g., Coupled Model Intercomparison Project phase 6, CMIP6 model) (D. Li et al., 2022; Taylor et al., 2012). The horizontal resolution of CMs typically ranges from 50 to 25 km (e.g., Flexible Global Ocean-Atmosphere-Land System Finite-Volume version 3, FGOALS-f3 model)(J. Li et al., 2021). The horizontal resolution of Me-WMs (e.g., The Global/Regional Assimilation Prediction System, GRAPES model, Weather Research and Forecasting, WRF model)(García-García et al., 2022; Ma et al., 2018) can be as fine as 1 km. The Mi-FMs can have a horizontal resolution of less than 100 m (e.g., Large eddy simulation, LES model)(Zhou et al., 2017). Studies have shown that the interaction between large- and small-scales is influenced by resolution, with finer resolution allowing for better characterization of underlying surface features and extreme events(Rummukainen, 2016; Singh et al., 2021), and also impacting future climate predictions(Chang et al., 2020; Roberts et al., 2020; Small et al., 2014). The use of PBL scheme is usually in coarse resolution models, which can lead to additional errors since these schemes are developed for flat terrain conditions(Weigel et al., 2007).

Finer vertical resolution can better capture changes in PBL structures, which can also have an impact on mass transport(Menut et al., 2013; O'Dea et al., 2017; Teixeira et al., 2016), especially on the accuracy of wind resources (Tolentino et al., 2016). In addition, horizontal and vertical resolutions can cause spurious gravity waves and increase model errors(Nolan and Onderlinde, 2022). Although finer resolution is better, there is no doubt that it is computationally expensive. Whether the use of finer resolution will bring significant improvement to the model results deserves further discussion. Different PBL schemes are combined with the different N-S schemes, both of which are crucial to the simulation results of the meteorological fields(Jia and Zhang, 2020). For instance, the MYJ PBL scheme can only couple the Eta N-S scheme, while the BL PBL scheme can couple both the MM5 and the Eta N-S schemes. The N-S scheme is pivotal for mesoscale numerical simulation, especially for fine numerical forecasting(Y. Li et al., 2010). Then, to figure out which scheme has a greater impact on the meteorological field will help to make targeted improvements to the forecasts in the future.

In addition, the lag of the underlying surface data can also affect the simulation results of the meteorological fields, especially for large cities with relatively rapid urbanization (Qian et al., 2022).

92 In particular, different underlying surface conditions can have different albedos that affect the

93 temperature changes, which can affect the urban heat island effect from a local perspective and

94 global warming from a global perspective.(Ouyang et al., 2022; Schwaab et al., 2021; Wang and Li,

95 2021).

96 The most commonly used final (FNL) reanalysis dataset is jointly produced by the National Centers

97 for Environmental Prediction (NCEP) and the National Center for Atmospheric Research (NCAR).

98 They have adopted a global data assimilation system and a well-established database for quality

99 control and assimilation of observations from various sources (ground, ships, radio soundings, wind

100 balloons, aircraft, satellites, etc.) to obtain a complete set of reanalysis dataset. The European Center

101 for Medium-Range Weather Forecasting (ECMWF, hereafter referred to as EC) has concluded that

102 the steady progress in numerical forecasting over the last 30 years is mainly attributed to

103 improvements in the forecast models themselves, the application of more observations and the

104 development of data assimilation techniques(Magnusson and Källén, 2013). Among them, the

105 performance of the forecast model depends largely on the model resolution, the accuracy of the

106 finite difference method, and the representativeness of the physical process parameterization

107 scheme. Different initial fields also influence the model results due to different observational data,

108 quality control methods, assimilation schemes, and bias correction methods adopted for different

109 reanalysis data(Ma et al., 2021).

110 Finally, we also have to take the update of the model version into account. With model versions

111 being updated, many parameterization schemes are more or less updated(Morichetti et al., 2022).

112 However, under the circumstance that the updates are not disclosed in scientific and technical reports

113 or papers, we need to dig into them from the code itself. In reality, simulation results will be likely

114 to vary from scholar to scholar because of different model versions they choose(Jia and Zhang,

115 2020). Consequently, it is necessary to adopt a control variable approach when discussing the impact

116 of model version updates. Instead of updating all parameterization schemes, only by updating the

117 ones we are concerned with can the uncertainty arising from version updates can be quantified.

118 These aforementioned uncertainties have been studied by scholars individually, but few scholars

119 have been able to synthesize and analyze these factors. In this part (i.e., Part II), each of these

120 uncertainties will be analyzed and discussed, and the factors with more significant effects will be

121 selected for reference in that identifying which factors besides the PBL scheme are critical to the

122 simulation of meteorological fields makes all the difference.

123   **2. Data and Methodology**

124   **2.1 Data**

125   **2.1.1 Reanalysis Data**

126   *Final (FNL) reanalysis data.* The NCEP global FNL reanalysis data are based on the 6 h

127   temporal resolution (i.e., 00:00 (08:00), 06:00 (14:00), 12:00 (18:00), 18:00 (02:00) UTC (BJT))

128   by the Global Data Assimilation System (GDAS) with a resolution of $1^{\circ} \times 1^{\circ}$ or $0.25^{\circ} \times 0.25$

129 $^{\circ}$. This product continuously collects observational data from the Global Telecommunications

130   System (GTS) and other sources. The FNL reanalysis data are made with the same model as

131   NCEP uses in the Global Forecast System (GFS), but the FNL reanalysis data are prepared

132   about an hour or so after the GFS is initialized. The FNL reanalysis data parameters include

133   surface pressure, sea level pressure, geopotential height, temperature, sea surface temperature,

134   soil values, ice cover, relative humidity, winds, vorticity etc. The data temporal range for 1-

135   degree is from July 30, 1999 to the present (https://rda.ucar.edu/datasets/ds083.2/), while the

136   time range for the 0.25-degree is from July 8, 2015 to the present

137   (https://rda.ucar.edu/datasets/ds083.3/).

138   *The fifth generation ECMWF reanalysis (ERA5) data.* The ERA5 is the fifth generation EC

139   reanalysis of the global climate. Reanalysis combines model data with observations worldwide

140   to form a globally complete and consistent dataset. ERA5 replaces its predecessor, the ERA-

141   Interim reanalysis. ERA5 data is available from 1959 to present with a resolution of $0.25^{\circ} \times$

142 0.25° (atmosphere) and $0.5^{\circ} \times 0.5^{\circ}$ (ocean waves). The model requires 3D data and 2D data,

143   and the variables of 3D data are temperature, U and V components of wind, geopotential height,

144   relative humidity (https://cds.climate.copernicus.eu/cdsapp#!/dataset/reanalysis-era5-pressure-

145   levels?tab=overview). The 2D data mainly includes the parameters surface pressure, mean sea

146   level pressure, skin temperature, 2-m temperature, 2-m relative humidity, 10-m U and V

147   components of wind, soil data and soil height

148   (https://cds.climate.copernicus.eu/cdsapp#!/dataset/reanalysis-era5-single-

149   levels?tab=overview).

150   **2.1.2 Underlying surface data**

151   The default underlying surface data in WRF are USGS and MODIS data, where USGS has 24

classifications and MODIS has 20 classifications. In this study, MODIS data is selected. The basic land cover is a modified International Geosphere Biosphere Programmer (IGBP), which is calculated by supervised classification using MODIS Terra and Aqua reflectance data, with a resolution of 500 m (https://www2.mmm.ucar.edu/wrf/users/download/get_sources_wps_geog.html). The dataset that comes with WRF is based on the year 2001(Bhati and Mohan, 2016). The 20 types are evergreen needleleaf, evergreen broadleaf, deciduous needleleaf, deciduous broadleaf, mixed forest, closed shrublands, open shrublands, woody savannas, savannas, grasslands, permanent wetlands, croplands, urban and built-up, cropland mosaics, snow and ice, bare soil and rocks, water bodies, wooded tundra, mixed tundra and barren tundra.

To consider the influence of the underlying surface data on the model results, we further select the same underlying surface data as the simulation period (i.e., January 2016) (https://e4ftl01.cr.usgs.gov/MOTA/MCD12Q1.006/). This data is MCD12Q1 version 6 data product(Friedl et al., 2002), including 17 land types that cover the IGBP land cover classification.

2.2 Description of the modelling experiments

The regional settings and basic settings of the model are the same as those in Part I, still for the five regions, and the month is selected as the test time only for January. To evaluate the effect of these uncertainties on the simulation results of the meteorological fields, a total of 12 experiments are conducted, and the detailed configuration of the experiments is shown in Table 1. The effect of horizontal resolution is presented by three experimental comparisons in Exp1, Exp2 and Exp3, and the effect of vertical resolution by Exp3 and Exp4. The implications of the surface layer schemes are analyzed by comparing three experiments in Exp5, Exp6 and Exp7. The impact of the initial field and boundary conditions are compared by three experiments, i.e., Exp3, Exp8 and Exp9. The influences of the underlying surface are displayed by two Exp3 and Exp10. The update of the model version is compared by Exp11 and Exp12.

Table 1 Detail parameters setting of the 12 experiments

Experiments	Horizontal resolution	Vertical resolution	PBL schemes	N-S schemes	Initial field and boundary condition	Underlying surface	Version of Model
Exp1	**75 km**	48 levels	YSU	MM5	FNL-1 º	Modis-15s	WRF v3.9.1
Exp2	**15 km**	48 levels	YSU	MM5	FNL-1 º	Modis-15s	WRF v3.9.1
Exp3	**3 km**	48 levels	YSU	MM5	FNL-1 º	Modis-15s	WRF v3.9.1
Exp4	3 km	**62 levels**	YSU	MM5	FNL-1 º	Modis-15s	WRF v3.9.1
Exp5	3 km	48 levels	**BL**	**MM5**	FNL-1 º	Modis-15s	WRF v3.9.1
Exp6	3 km	48 levels	**MYJ**	**Eta**	FNL-1 º	Modis-15s	WRF v3.9.1
Exp7	3 km	48 levels	**BL**	**Eta**	FNL-1 º	Modis-15s	WRF v3.9.1
Exp8	3 km	48 levels	YSU	MM5	**FNL-0.25 º**	Modis-15s	WRF v3.9.1
Exp9	3 km	48 levels	YSU	MM5	**EC-0.25 º**	Modis-15s	WRF v3.9.1
Exp10	3 km	48 levels	YSU	MM5	FNL-1 º	**Modis-15s (2017)**	WRF v3.9.1
Exp11	3 km	48 levels	ACM2	MM5	FNL-1 º	Modis-15s	**WRF v3.9.1**
Exp12	3 km	48 levels	ACM2	MM5	FNL-1 º	Modis-15s	**WRF v3.6.1[+*]**

179 [*]WRF3.6.1[+] refers to the migration of the ACM2 scheme from WRFv3.6.1 to WRFv3.9.1, ensuring

180 that no changes in other parameterization schemes. Bold text indicates uncertainties of primary

181 concern.

182 **3 Results and discussion**

183 **3.1 horizontal resolution impact on 2-m temperature and 10-m wind speed**

184 The underlying surface information is crucial to the simulation of near-surface meteorological

185 parameters. From the distribution of the underlying surface, the three different resolutions of the

186 model can basically capture the general information of the underlying surface (Fig. 1). The

187 resolution of 75 km is relatively coarse, so many fine features are ignored and represented uniformly

188 by a large grid (Fig. 1a). The resolution of 15 km is very significantly different compared to 75 km

189 (Fig. 1b), and many fine characteristics (e.g., lakes, cities, etc.) are represented, very close to the

190 features of 3 km.
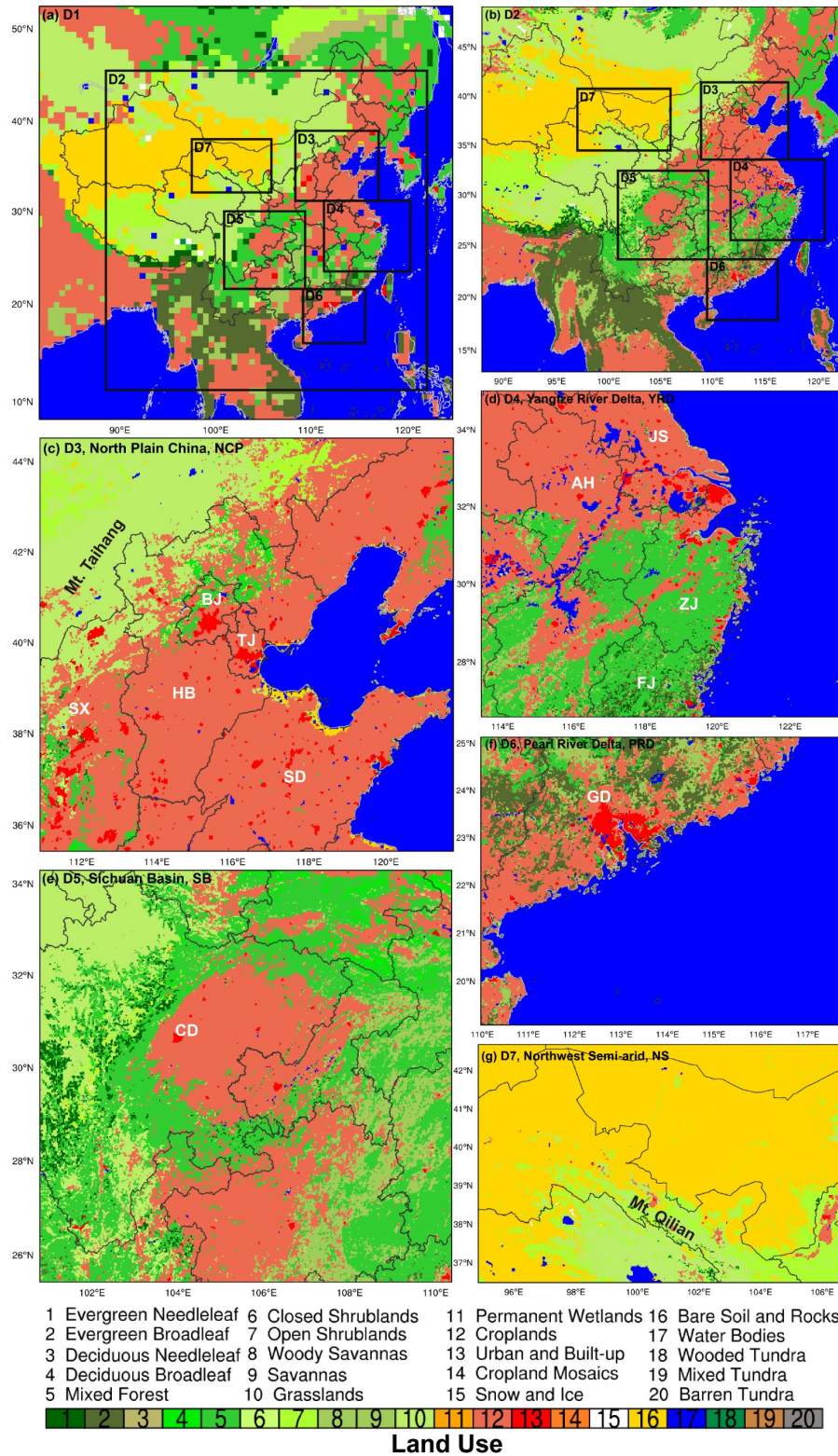
Land Use

Figure 1. (a-g) Map of land use type in the seven nested model domains. The abbreviations BJ, TJ, HB, SX, SD, JS, ZJ, AH, FJ, CD, GD, Mt. Taihang and Mt. Qilian are denoted as Beijing Shi, Tianjin Shi, Hebei province, Shanxi province, Shandong province, Jiangsu province, Zhejiang province, Anhui province, Fujian province, Chengdu Shi, Guangdong province, Taihang mountains and Qilian mountains in figure c-g, respectively.

Further comparative analysis of temperature and wind speed in five regions at these three resolutions have been performed. In terms of regional distribution, all three experiments can simulate high and low value areas of 2-m temperature, but there are differences in the degree of overestimation and underestimation (Fig. 2). In the NCP region, the three experiments underestimate the temperature over a similar range of regions, especially in the northwest (Fig. 2a1-c1). Experiment 1 differs more sharply from the other two experiments in areas with more marked underlying surface variability such as in the complex mountainous areas (i.e., Taihang mountains, Mt. Taihang) in the northwest, the underestimation of Exp1 is more significant, but at the sea-land interface, the overestimation of Exp1 is more pronounced (Fig. 2a1), because the grid resolution is too low. The number (N) of stations overestimated by the three experiments is 96, 128 and 172, and the relative bias (RB) are 0.38%, 0.19% and 0.18%, respectively. Although the number of stations overestimated by Exp1 is small, there are more extreme values, so the deviation is larger. Correspondingly, the higher degree of underestimation (-0.89%) in Exp1 derives from more minimal values and stations (N=397) as well. For the YRD region, obviously, Fig. 2a2-c2 note that the RB of the stations vary greatly with different horizontal resolutions, especially for the northeastern coastal of YRD region (i.e., northeast Jiangsu (JS) province) from overestimation (Fig. 2a2) to underestimation (Fig. 2c2), and the degree of underestimation gradually decreases in the southeast of YRD (i.e., Zhejiang (ZJ) and Fujian (FJ) provinces). In the SB region, it is clear that Exp1 underestimates the 2-m temperature more significantly (RB=-1.11%, N=245), with fewer stations in the fig. 2a3, followed by Exp2 (RB=-1.03%, N=208), and to a lesser extent by Exp3 (RB=-0.69%, N=152). The PRD region behaves differently from other regions, with the simulation results of Exp1 showing an underestimation (RB=-0.11%), while Exp2 (RB=0.13%) and Exp3 (RB=0.35%) an overestimation (Fig. 2a4-c4). The variation of underlying surface between grids in the PRD region is more complex in comparison with other regions (Fig. 1). This does not indicate that the simulation results are better when the grid horizontal resolution is lower, because the scheme itself still has errors in the simulation. It only reveals that the simulation results of Exp1 perform better statistically in the current model configuration for this region. The number of stations in Exp1 in the NS region is much less than the other two experiments, which means that the relative bias of Exp1 is more than ±3% and the deviation is greater, for the area along the Qilian mountains (Mt. Qilian) (Fig. 2a5-c5) in particular. The results of wind speed are different from those of temperature, and the difference between the three experiments is not as obvious as that of temperature (Fig. 3). The three experiments

228 overestimate the wind speed to varying degrees, however, more stations underestimate wind speed

229 in the Exp1, especially in the NCP (N_{Exp1}=34, N_{Exp2}=21, N_{Exp3}=19) and SB region (N_{Exp1}=29,

230 N_{Exp2}=18, N_{Exp3}=7) (Fig. 3a3). As the grid resolution is too coarse in the Exp1, the wind speed is

231 underestimated at some stations due to the complex terrain in the NCP and SB regions (Fig. 3a1,

232 a3).
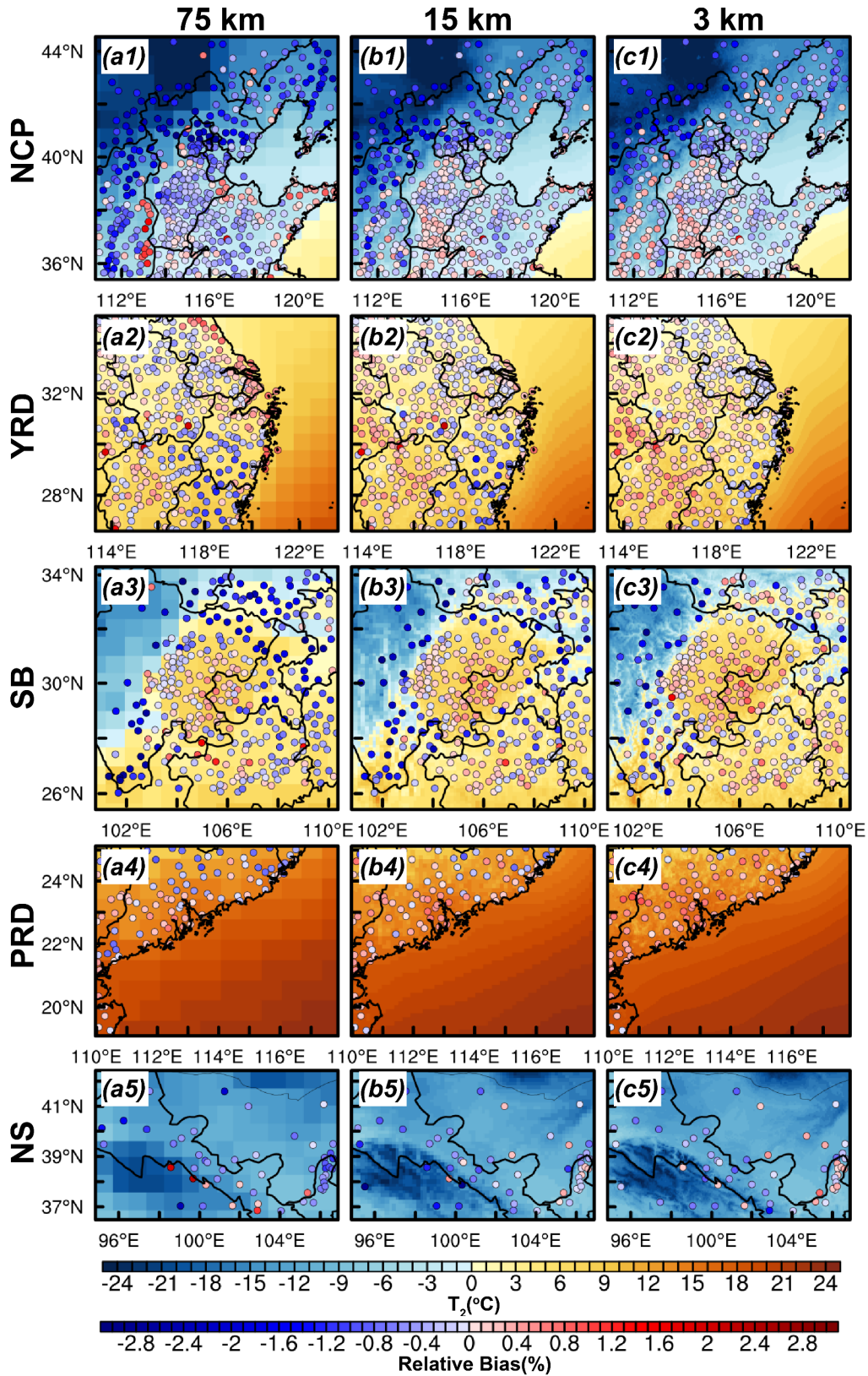
Figure 2. Regional distribution of 2-m temperature simulated by the (a) domain 1 (75 km), (b) domain 2 (15 km) and (c) domain 3 (3 km) for five regions in January, and distribution of relative bias between simulations and observations is denoted by scatters.

237 It can also be seen from figure 4 that the three experiments have a large difference in temperature

238 simulation, and the underestimate in Exp1 is more significant (Fig. 4a1-a5). However, in the PRD

239 region, the average value of the mean bias is closer to 0 on account of the offsetting positive and

240 negative deviations. For the distribution range of the mean bias, it has been found that the

241 distribution of the Exp1 is closer to 0 (Fig. 4a4). In terms of the cumulative probability distribution,

242 the simulations differ for different temperature segments in the NCP, SB, and NS regions. For the

243 NCP region, the temperature below 270 K is better simulated in Exp3, the temperature threshold in

244 the SB region is about 280 K, and the threshold is about 265 K in the NS region (Fig. 4b1, b3, b5).

245 In the YRD region, the simulations of all three experiments are almost the same for any segmented

246 temperature (Fig. 4b2). In addition, the PRD region is special, with temperature below about 285 K,

247 and the Exp2 simulates better (Fig. 4b4). It is worth noting that, regardless of the region, one thing

248 in common is that the temperature of the three experiments simulations gets closer and closer as the

249 temperature increases. While the difference of wind speed between the three experiments is not

250 obvious (Fig. 4c1-c5). The average value of the mean bias in Exp1 is closer to 0, mainly attributable

251 to that there are more stations with negative mean bias to offset. Wind speed and temperature behave

252 differently in regard of cumulative probability distributions, with increasing differences in simulated

253 wind speeds for the three experiments as wind speed increases (Fig. 4d1-d5). The wind speed

254 simulated in Exp1 is low, leading to a better performance in Exp1 for small wind speed (Fig. 4d1-

255 d5).
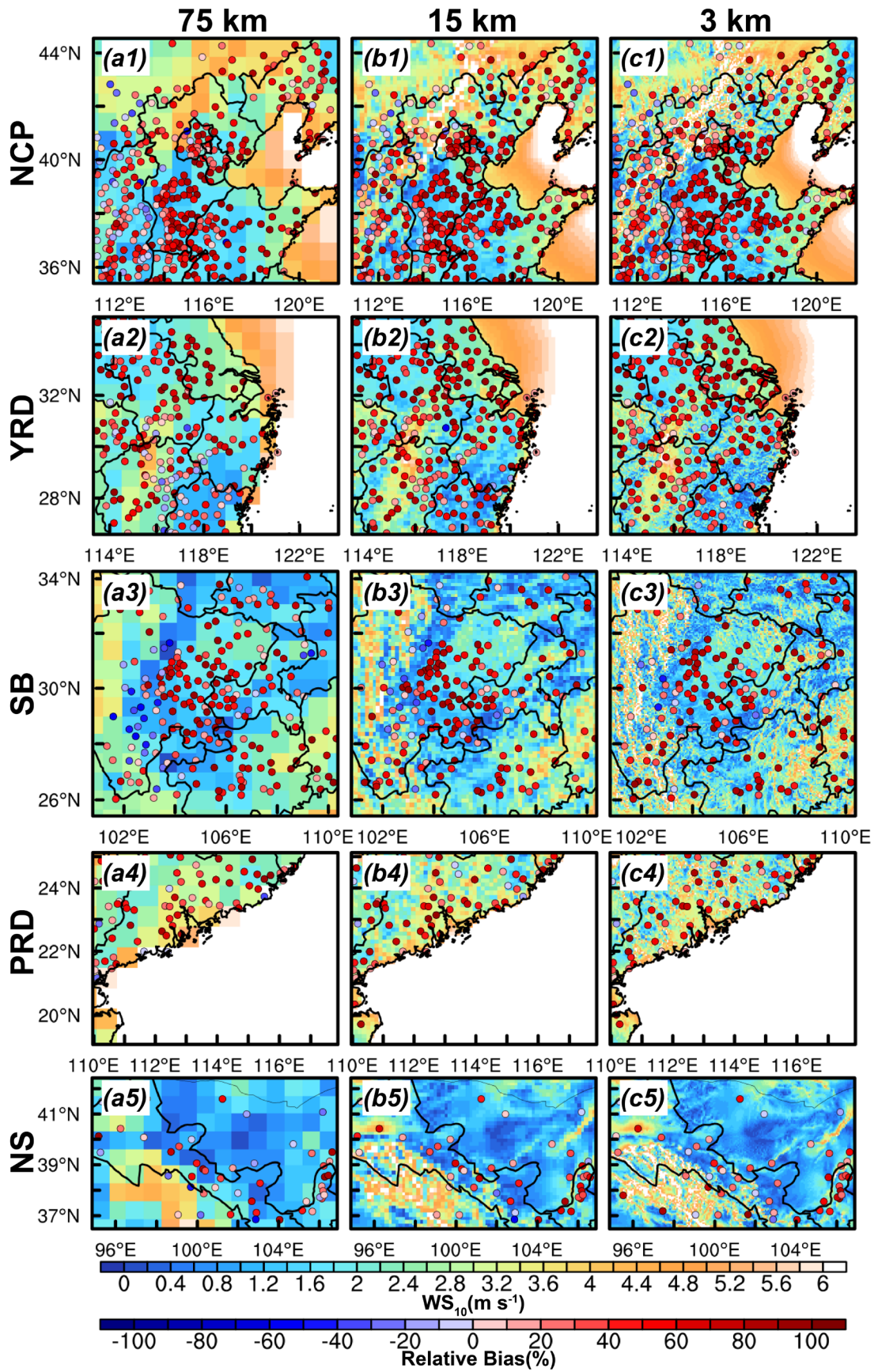
256

257 Figure 3. Similar as figure 2, but for 10-m wind speed.

258
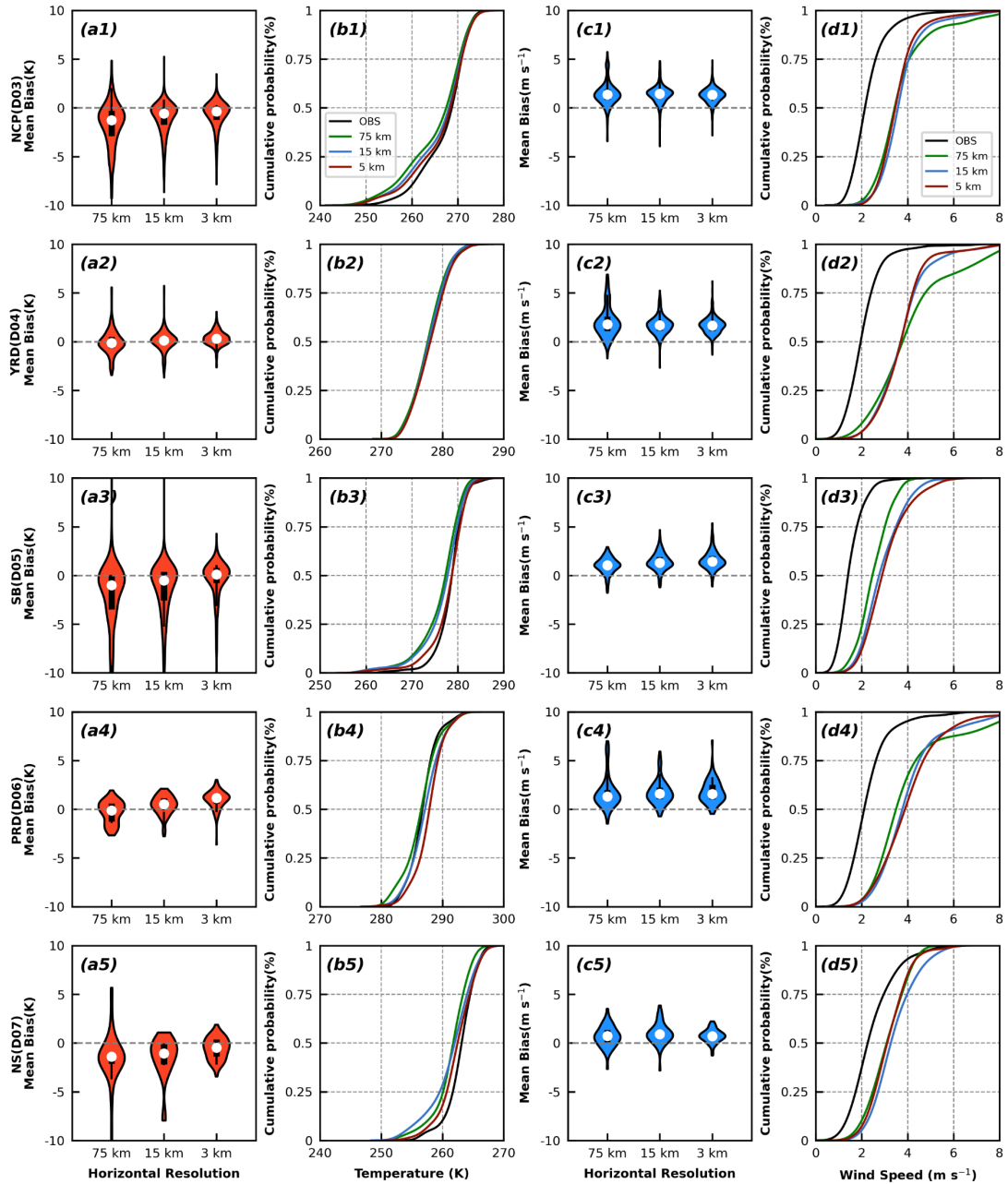
259 Figure 4. Violin-plots of mean bias of observed and simulated (a1-a5) 2-m temperature and (c1-c5)

260 10-m wind speed at different horizontal resolution (i.e., 75 km, 15 km, 3 km), cumulative

261 probability of observed and simulated (b1-b5) 2-m temperature and (d1-d5) 10-m wind speed at

262 different horizontal resolution (i.e., 75 km, 15 km, 3 km) for five regions.

263 **3.2 vertical resolution impact on PBL structures**

264 Based on Exp3, the vertical resolution has been further encrypted from 21 to 35 levels below 2 km,

265 i.e., the total number of vertical levels is increased from 48 to 62 levels (Fig. 5). The temperature

266 and wind fields of the two experiments (Exp3 and Exp4) simulations are compared for the four

267 sounding stations selected for each region in Part I (NCP: Beijing, Zhangjiakou, Xingtai and
268 Zhangqiu; YRD: Anqing, Nanjing, Shanghai and Quzhou; SB: Hongyuan, Wenjiang, Shapingba and
269 Daxian; PRD: Qingyuan, Shantou, Yangjiang and Heyuan; NS: Mazongshan, Jiuquan, Zhangye and
270 Minqin). As can be seen from figure 6, the re-encryption of the vertical resolution has no effect on
271 the simulation of the temperature, regardless of the region. The simulation results of the two
272 experiments almost overlap in the vertical direction, implying that the vertical structure of 48 levels
273 is sufficient. On the contrary, the encryption of vertical resolution affects the simulation results of
274 wind speed to a certain extent, but the effect is marginal, especially for high altitude regions like SB
275 and NS (Fig. 7). For the YRD and PRD regions, the wind speed simulated in Exp4 is less than that
276 of Exp3 below 1000 m, with a difference of less than 1 m s^{-1}. However, the encryption of the vertical
277 resolution causes an increase in memory, which would add about 5 GB of memory for a region of
278 1-day results, and the 150 GB for a month. Therefore, the improvement in wind speed in some areas,
279 due to the increase in vertical resolution, is not worth the cost of increased memory, as the
280 improvement is simply too insignificant.
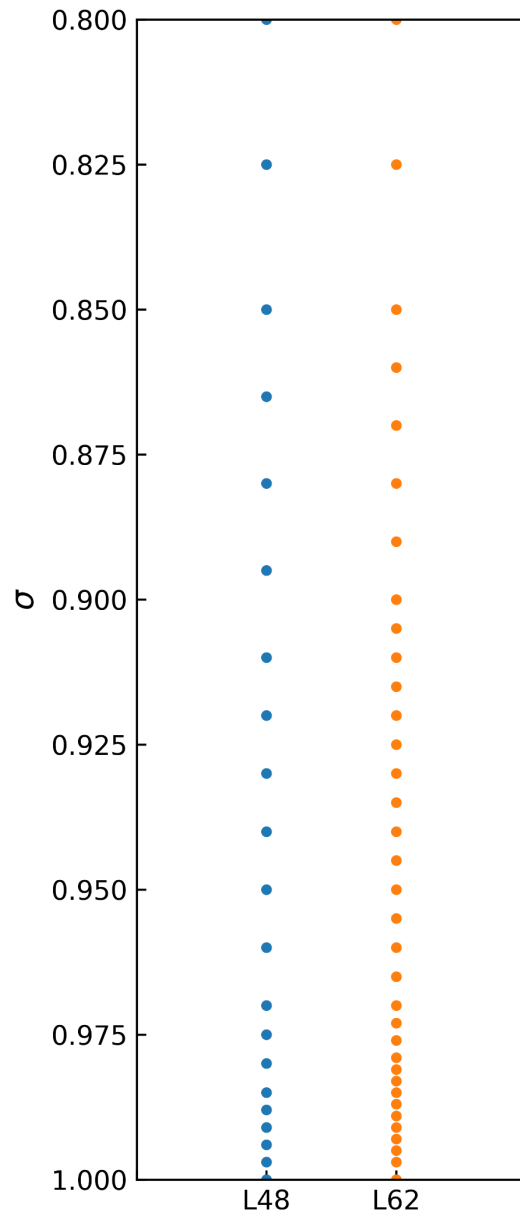
281

282 Figure 5. Vertical levels distribution for the two experiments of σ below 2 km in the model.

283
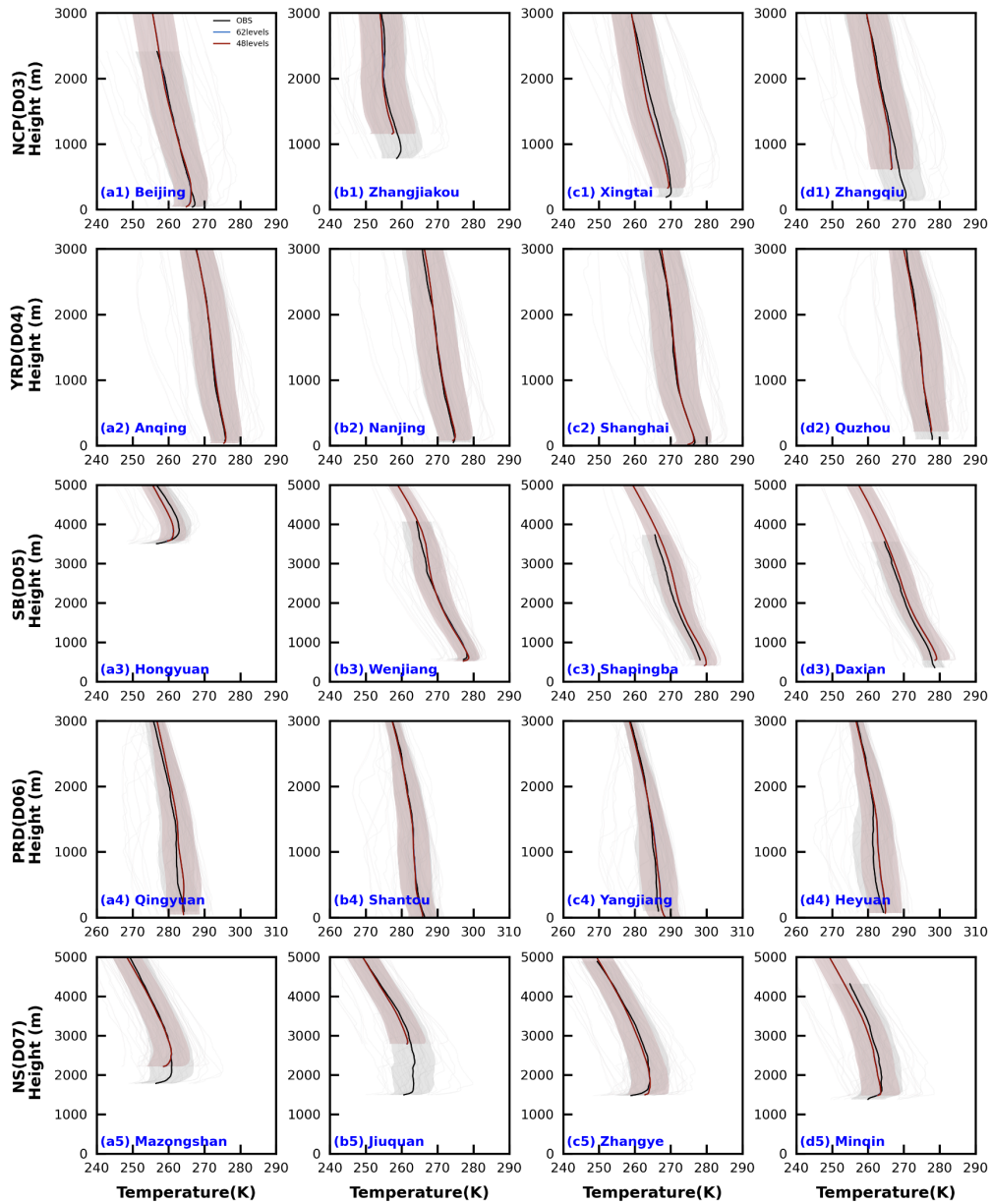
284 Figure 6. Average vertical profiles of observed and simulated temperature at 08:00 and 20:00 BJT

285 at four sounding stations for each region in January. The unobtrusive gray lines indicate the

286 simulated lines for all time periods, and the lines with shading indicate the average values and

287 shaded areas show the uncertainty range (the mean ±1 standard deviation).
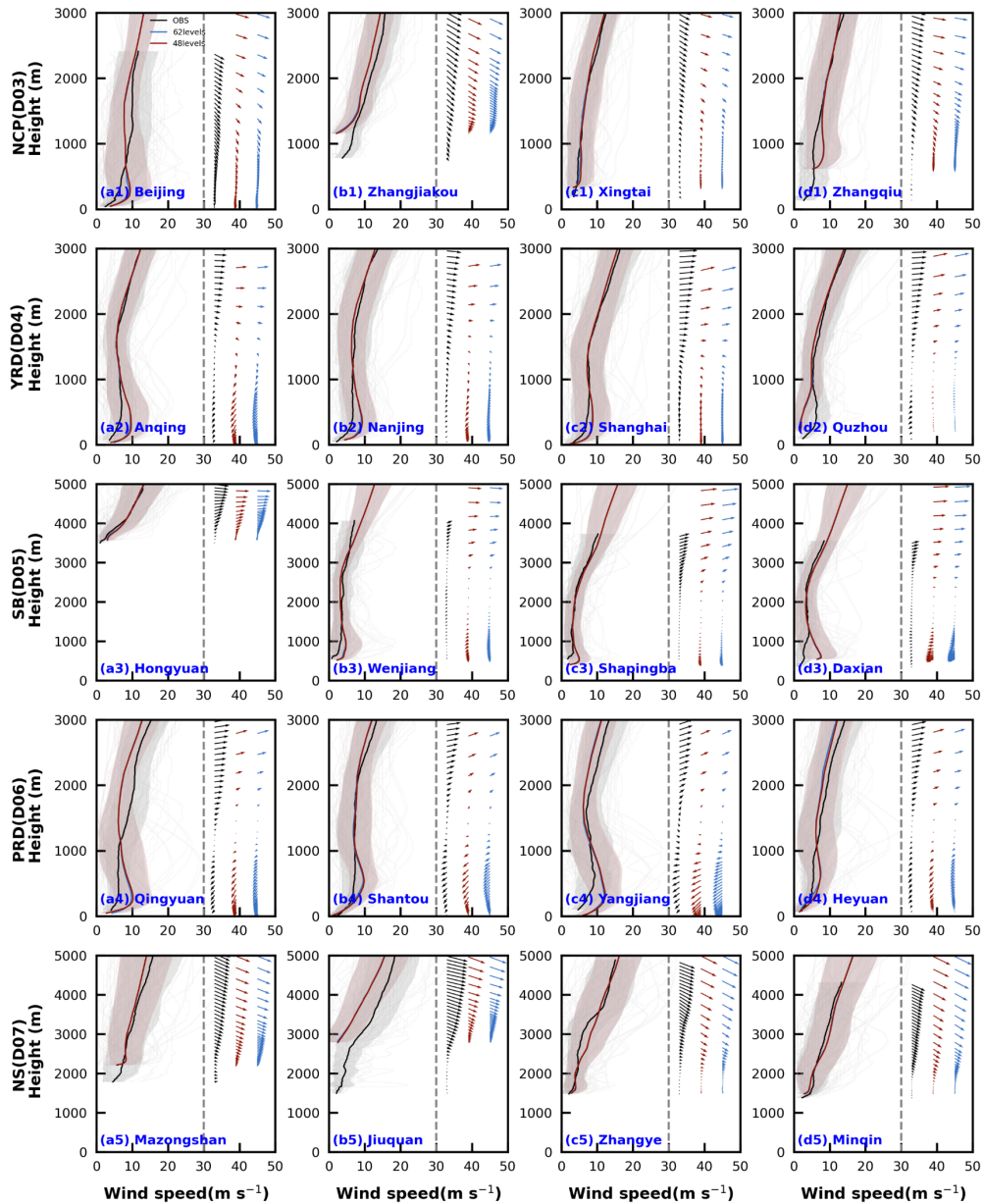
Figure 7. Similar as figure 6, but for wind speed and direction.

It is not necessary to set the vertical resolution much finer compared to the horizontal resolution, and in this experiment, 48 levels are fully sufficient to reproduce the vertical structure of the PBL.

3.3 near-surface (N-S) scheme impact on PBL structures

For the impact of the N-S scheme, this section focuses on the changes in the N-S meteorological parameters.

The N-S and PBL schemes are fixed pairings, and three experiments (i.e., Exp5, Exp6 and Exp7) are done by this study to distinguish the extent to which the N-S and PBL schemes affect the N-S meteorological parameters (2-m temperature, 2-m relative humidity, 10-m wind speed and direction).

298 In terms of daily variation, the variation of temperature in the five regions is consistent, with similar

299 simulated results in Exp5 (BL+MM5) and Exp7 (BL+Eta), and two experiments have notable

300 differences from Exp6 (MYJ+Eta) (Fig. 8a1-a5). However, the relative humidity and temperature

301 are different, and the results of Exp5 and Exp7 are not close to each other (Fig. 8b1-b5). From the

302 results of wind speed, it is similar to the results of temperature, and the results of Exp5 and Exp7

303 are much closer, as is the wind direction (Fig. 8c1-d5). Furthermore, the three schemes are made

304 differential to quantify the impact of the PBL scheme and N-S scheme. Exp6-Exp7 note the impact

305 of the PBL scheme, and Exp5-Exp7 illustrate the effect of the N-S scheme.
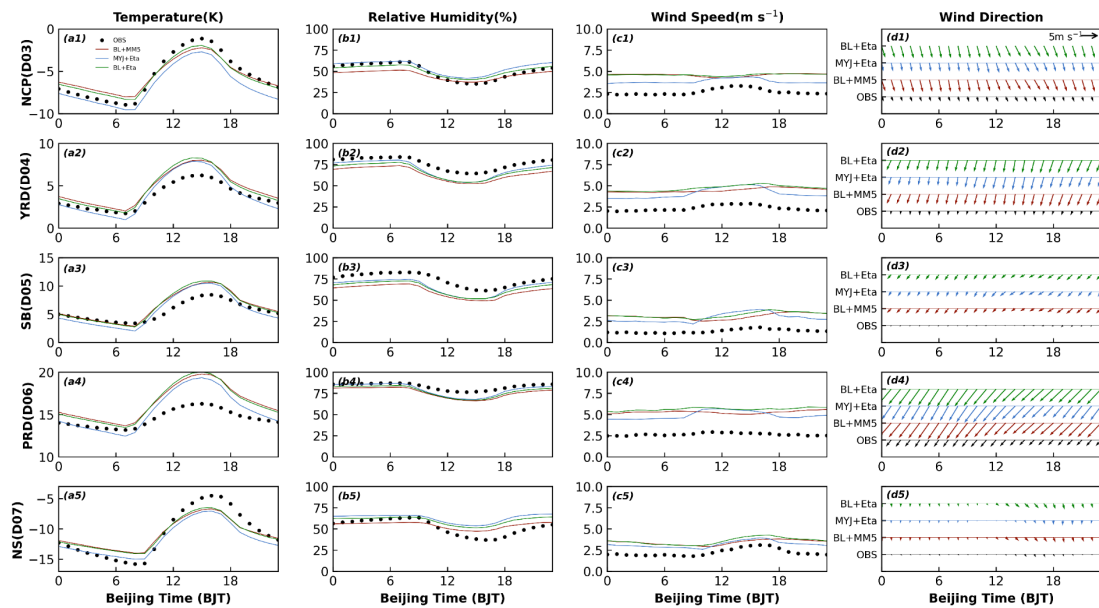
306

307 **Figure 8. Time series of diurnal variation of (a1-a5) 2-m temperature, (b1-b5) 2-m relative**
308 **humidity, (c1-c5) 10-m wind speed and (d1-d5) 10-m wind direction for five regions in January.**

309 As can be seen from fig. 9a1-a5, the influence of the PBL scheme is greater compared to the N-S

310 scheme in five regions. The difference in temperature simulated by different PBL schemes is about

311 1 K, while the difference for N-S schemes is just less than 0.5 K. In figure 9b1-b5, as in figure 8,

312 the results for relative humidity differ from those for temperature. The PBL scheme does not affect

313 the relative humidity to the same extent as the N-S scheme, and it is also less than the N-S scheme.

314 Particularly in the NCP, SB, and NS regions, the impact of the PBL scheme is much smaller than

315 that of the N-S scheme (Fig. 9b1, b3, b5). Regardless of the PBL scheme and N-S scheme, the effect

316 is greater at night than during the day. The findings for wind speed and temperature are more similar,

317 with the PBL scheme having a remarkably greater impact than the N-S scheme (Fig. 9c1-c5). Except

318 for the daytime in both YRD and PRD regions, the N-S scheme has a slightly greater effect on wind

319 speed than the PBL scheme (Fig. 9c2, c4). The wind direction is divided into a total of eight

320 directions (N, N-E, E, S-E, S, S-W, W, N-W), and the influence of the PBL scheme is larger as to

321 the percentage frequency of each direction (Fig. 9 d1-d5).
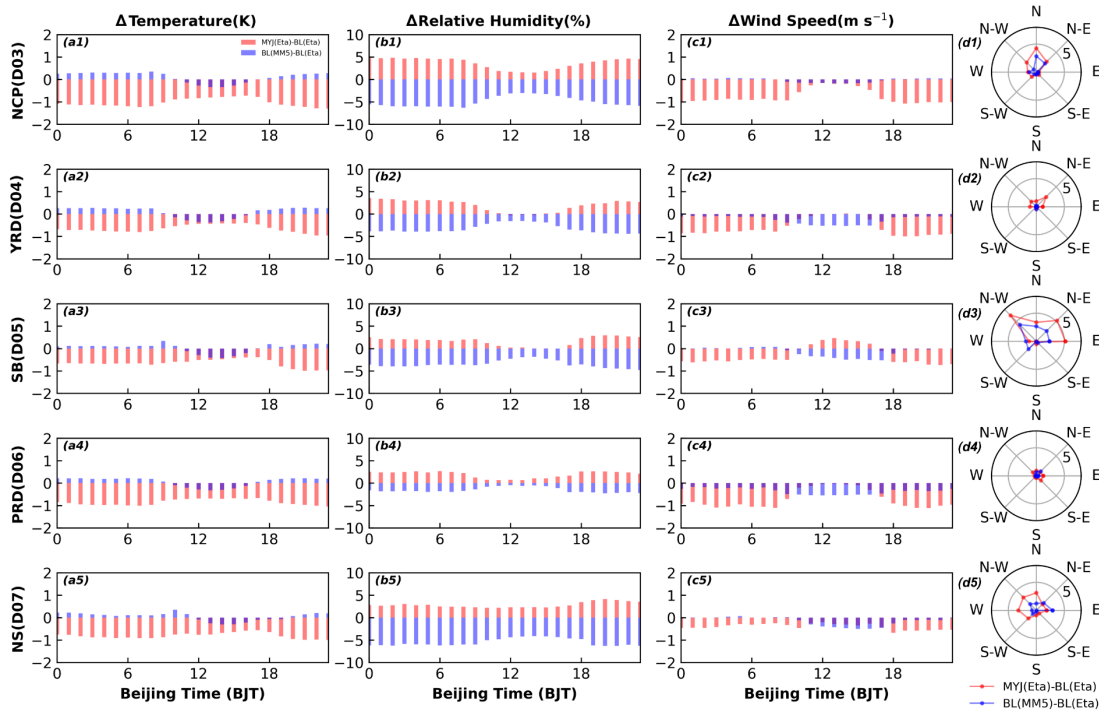
322

323 **Figure 9. Time series of diurnal variation of the effects of PBL scheme and N-S scheme on (a1-a5)**

324 **2-m temperature, (b1-b5) 2-m relative humidity, (c1-c5) 10-m wind speed and (d1-d5) 10-m wind**

325 **direction for five regions in January.**

326 As for the regional distribution of temperatures, the distribution of Exp5 and Exp7 is more similar,

327 without regard to the region, and it differs considerably from that of Exp6 (Fig. 10). Therefore, for

328 temperature, the effect of the PBL scheme is more important. For wind speed, Exp7 simulates the

329 largest wind speed, followed by Exp5, and Exp6 has the smallest wind speed, noting that the PBL

330 scheme has a larger degree of influence than the N-S scheme (Fig. 11).
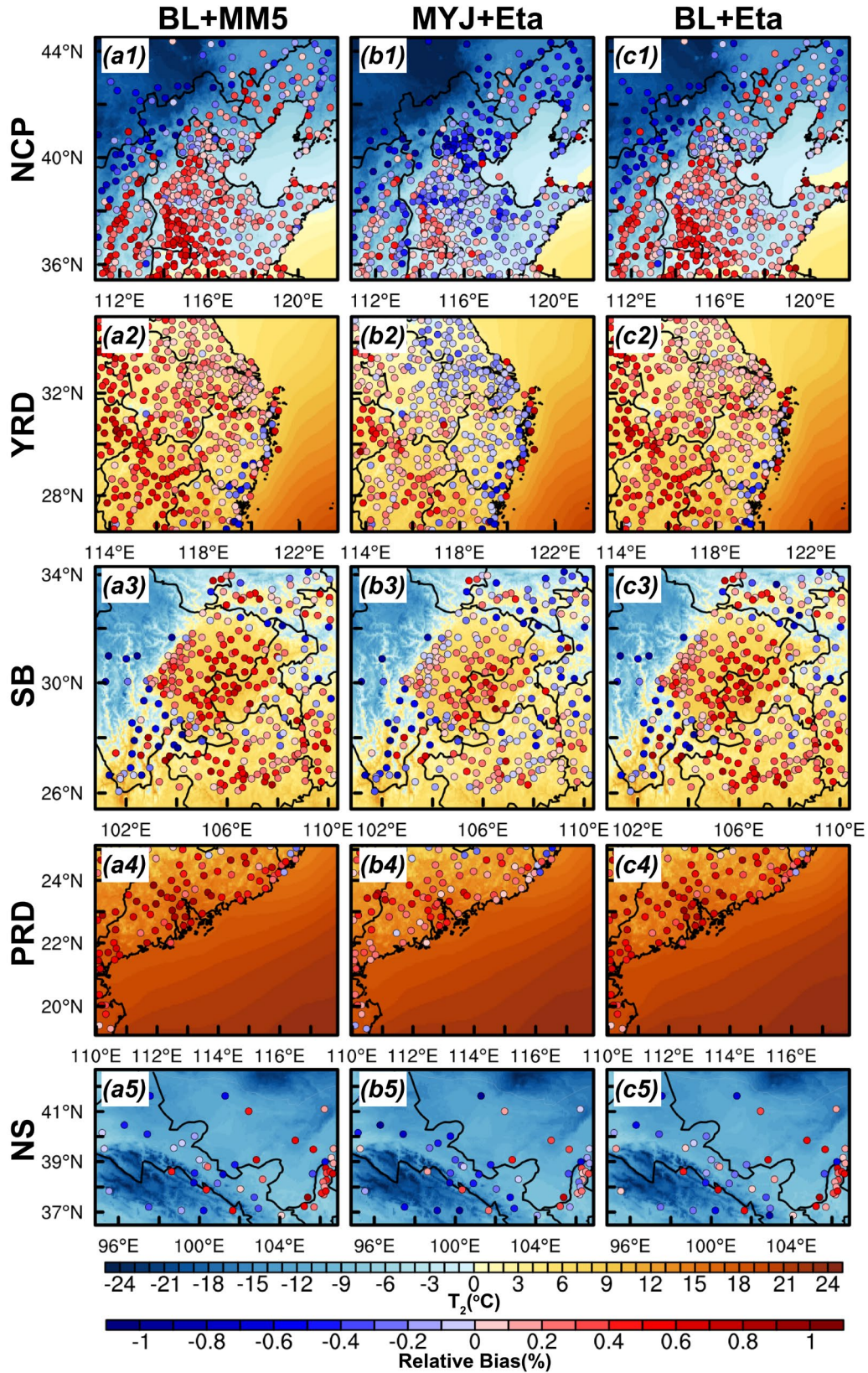
Figure 10. Regional distribution of 2-m temperature simulated by the (a) BL+MM5, (b) MYJ+Eta and (c) BL+Eta for five regions in January, and distribution of relative bias between simulations and observations is denoted by scatters.

335   In general, for temperature, the choice of PBL scheme is of much more importance. For relative

336   humidity, the PBL and N-S schemes are equally important, except for the NCP, SB and NS regions,

337   where the choice of the N-S scheme is more principal. For wind speed and direction, the choice of

338   PBL scheme is more critical, and the simulation of different PBL schemes leads to more differences

339   in the results.
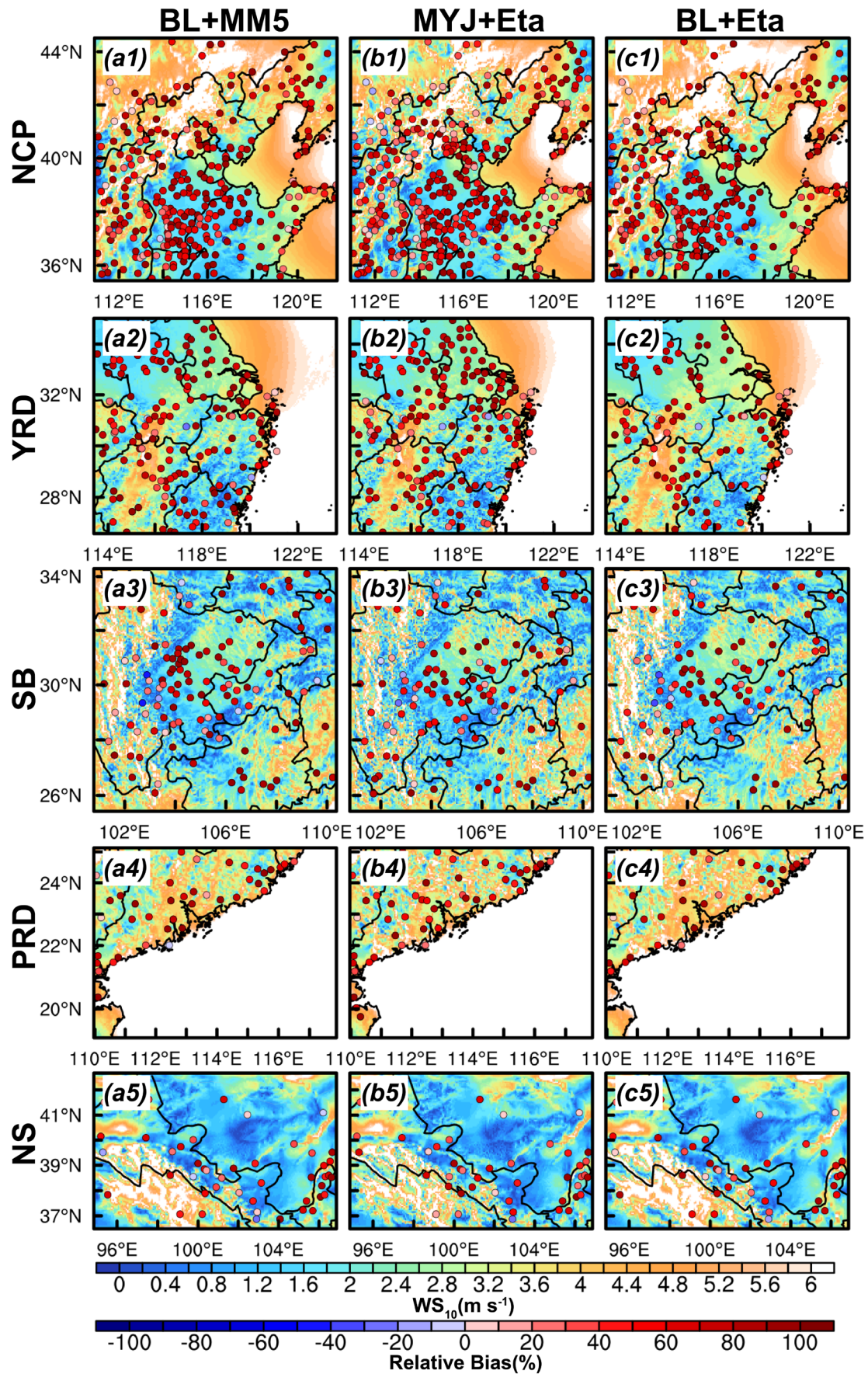
Figure 11. Similar as figure 10, but for 10-m wind speed.

342 **3.4 effect of initial and boundary conditions on meteorological parameters**

343 In this subsection, the same initial field and boundary conditions at different resolutions (i.e., FNL–

344 1° and FNL–0.25°) and different initial field and boundary conditions at the same resolution (i.e.,

345 FNL–0.25° and EC–0.25°) are chosen to explore the effects of the initial field and boundary

346 conditions on the meteorological field simulation. Figure 12 shows the daily variation series of 2-m

347 temperature, 2-m relative humidity and 10-m wind speed and direction. Also, figure 12 notes that

348 for temperature and relative humidity, the effect of data with different resolutions of the same initial

349 field on the results is small, but the effect of data with different initial fields of the same resolution

350 is profound. For the five regions, the EC data better simulate the temperature than the FNL data

351 during the day, while at night, the difference between the two types of data simulating the

352 temperature becomes less than during the day, except for the NCP and NS regions (where the

353 temperature difference is larger for both day and night) (Fig. 12 a1-a5). For relative humidity, the

354 EC data are simulated better than the FNL data regardless of the region, playing a key role in

355 improving the relative humidity results of the model (Fig. 12 b1-b5). Overall, the increase in

356 resolution of the initial field data from 1° to 0.25° has less effect on the simulation of temperature

357 and relative humidity, while there is a striking difference between the different initial field data.
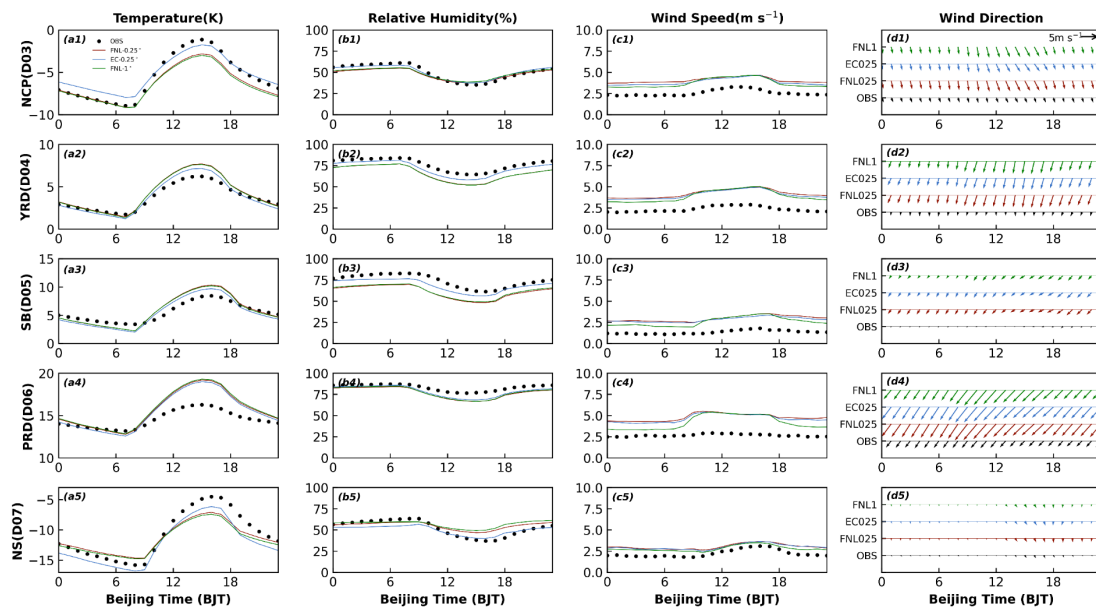
358

359 **Figure 12. Similar as figure 8, but for different initial and boundary conditions.**

360 The results for wind speed differ from the first two parameters in that there is almost no difference

361 between the three experiments for wind speed simulations during the day (Fig. 12 c1-c5). However,

362 different initial field data at the same resolution have very little effect on the wind speed, but the

363 same initial field data at different resolutions have a significant effect on the wind speed, especially

364 at night (Fig. 12c1-c5). All data have a negligible effect on the wind direction (Fig. 12 d1-d5).

365 The EC data have improved the results of relative humidity for all regions as mentioned earlier (Fig.

366 12 b1-b5). In terms of regional distribution, the regional distribution of FNL data is similar in shape

367 for different resolutions (Fig. 13 a, c). However, the relative humidity distribution simulated by EC

368 data and FNL data is drastically different (Fig. 13). It is worth noting that the relative humidity of

369 the EC data is the highest in the four regions except for the NS region in which the relative humidity

370 is the lowest (Fig. 13 b1-b5).
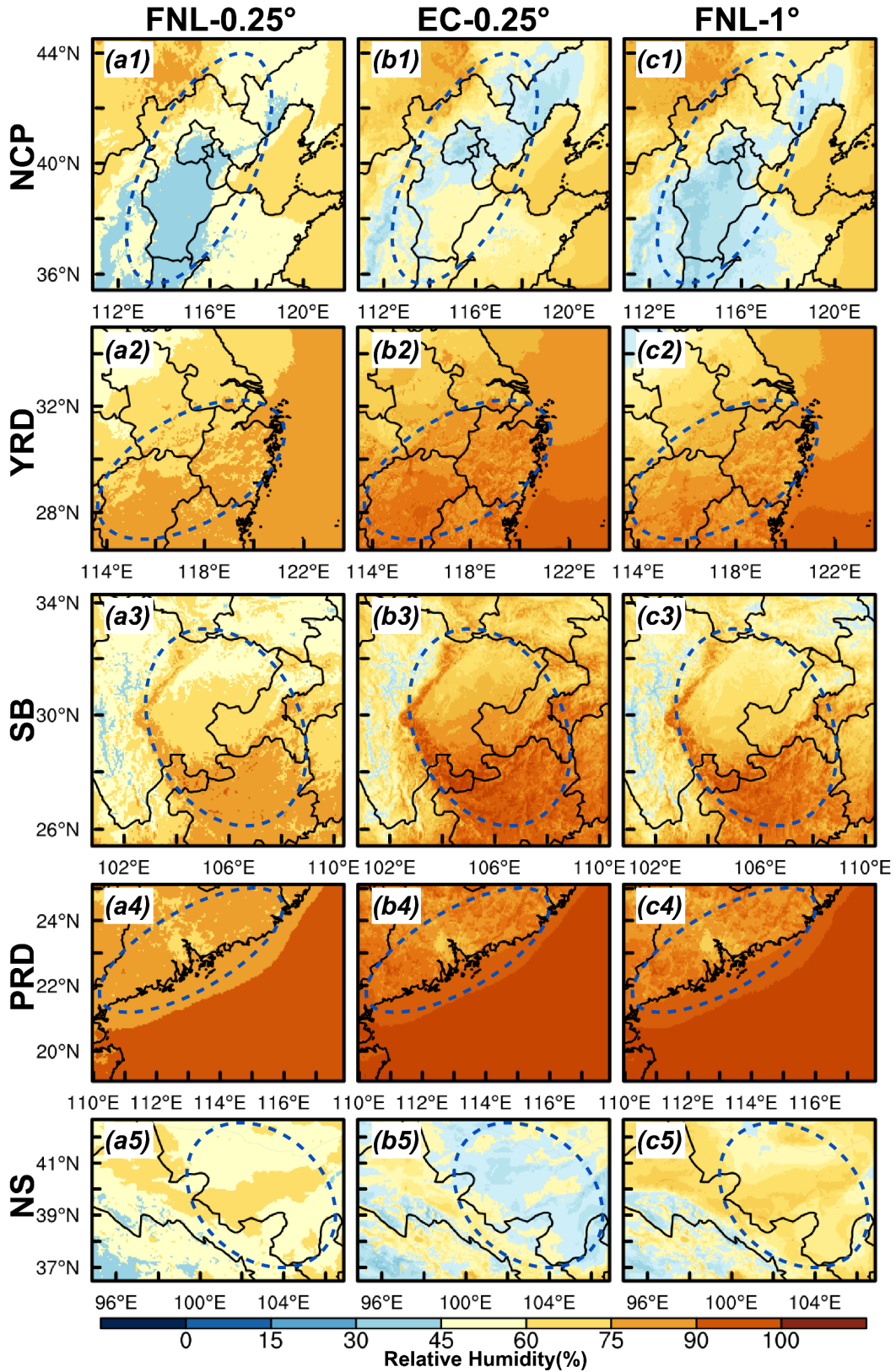
Figure 13. Regional distribution of 2-m relative humidity simulated by the (a) FNL-0.25°, (b) EC-0.25° and (c) FNL-1° for five regions in January, and the blue dashed circles indicate the regions where the results of the three experimental simulations differ significantly.

375   In the vertical direction, the simulated results of the three experiments for temperature and wind

376   speed do not differ much, unlike the near-surface meteorological parameters (i.e., T_2, RH_2, WS_{10}

377   and WD_{10}) that show such obvious differences (Fig. S1, S2). Nevertheless, for the relative humidity,

378   the variation in vertical direction at different heights is more consistent with the near-surface layer,

379   where the relative humidity of EC data is high in the whole layer (Fig. S3). Except for a few highland

380   stations outside the basin in the SB region, the relative humidity of EC data is low at higher altitudes

381   (Fig. S3 a3, b3, d3).

382   **3.5 effect of underlying surface on meteorological parameters**

383   To further explore the impact of underlying surface changes on the simulation results of

384   meteorological fields, we use the underlying surface data in January 2016 that is closer to the

385   simulation time, in addition to the default underlying surface data that comes with the model, for

386   comparative analysis of the simulation. Comparing figure 1 and figure 14, it can be concluded that

387   the most substantial change in the Domain 1 area is in the croplands type (i.e., code 12), especially

388   for the area south of latitude 30 °N. Many types with an underlying surface of 12 have become 14

389   or 8, 9 etc. Although both 12 and 14 here can represent cropland, there are some differences in the

390   specific descriptions. Code 12 mainly indicates that at least 60% of area is cultivated cropland, while

391   code 14 mainly refers to the mosaics of small-scale cultivation 40–60% with natural tree, shrub, or

392   herbaceous vegetation. In addition to croplands, the two types of urban and water bodies are more

393   variable as well. Therefore, this subsection focuses on the effects of urban and water body changes

394   on surface meteorological fields.
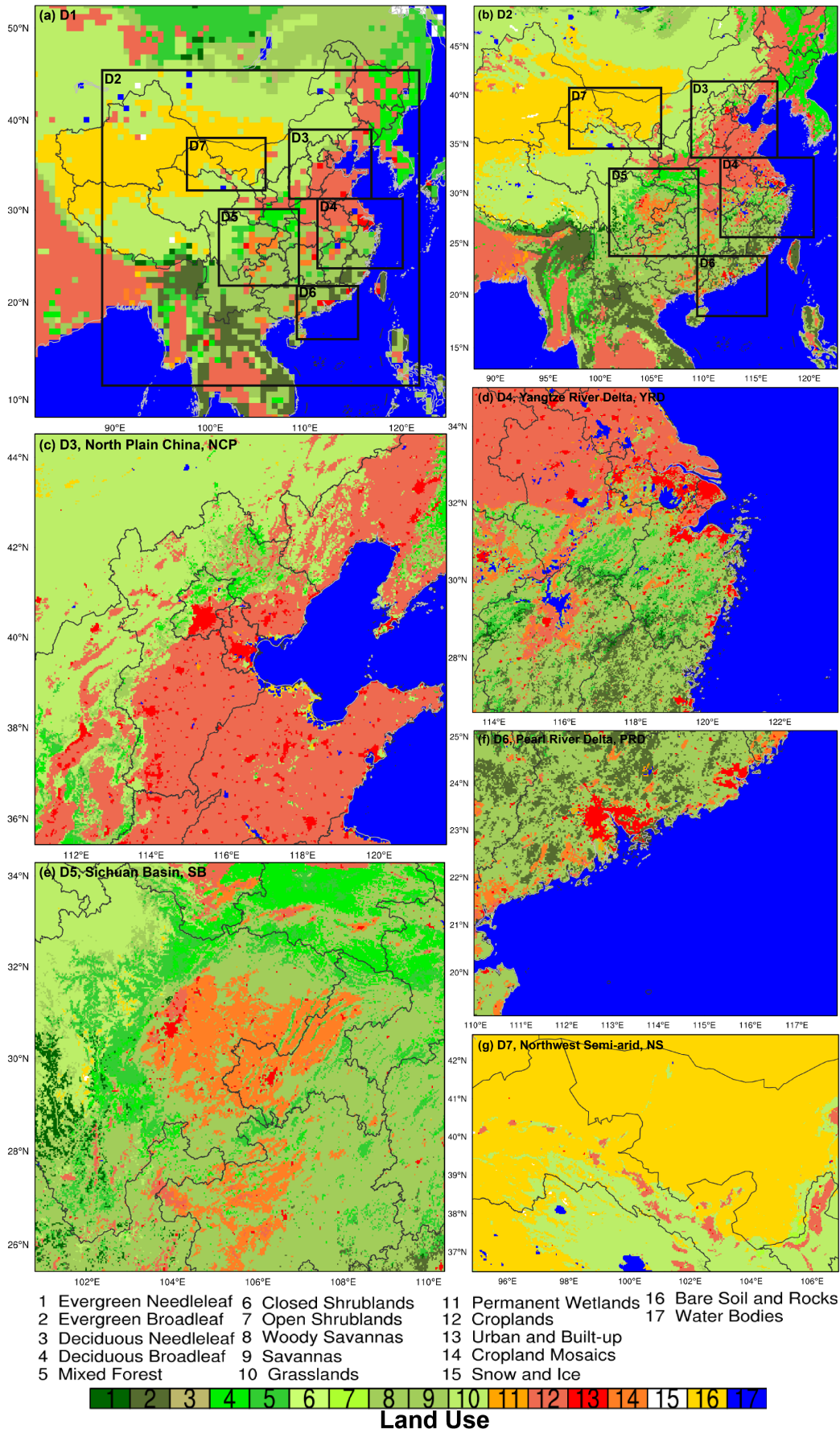
395

396 Figure 14. Similar as figure 1, but for the land use type for January 2016.

In terms of the overall regional distribution, the new underlying surface did not affect the areas of high and low values of temperature (Fig. 15 a-b) to an important degree. However, the difference between the simulation results of two different underlying surface shows that the change of the underlying surface has an effect on the temperature by about ±1 °C, especially for the grids with more obvious changes in water bodies and urban areas (Fig. 15 c). In the NCP region, an increase in the area of water bodies in the coastal areas of Tianjin (TJ) Shi, Shandong (SD) province, and Jiangsu (JS) province leads to a distinct increase in temperature (i.e., indicated by red boxes), while a decrease in the area of inland water in the northern region of Shanxi (SX) province causes a decrease in temperature (i.e., denoted by blue boxes) (Fig. 15 c1). The decrease in the area of water bodies in the Yangtze River in the YRD region has caused a decrease in temperature, while urbanization has contributed to an increase in temperature in several regions (Fig. 15 c2). The underlying surface changes in the SB region are mainly in the form of forest and savannas changes, as well as the more rapid urbanization of the provincial capital city of Chengdu (CD) Shi (Fig. 14 e). The development of this city has a positive feedback effect on the temperature of the region (Fig. 15 c3). The underlying surface change in the YRD region is from croplands to savannas, with a rapid greening rate, and its excessive greening may make the green coverage of some cities too high, leading some grids to identify the cities as savannas. In the NS region, the area of croplands and cities along the Qilian Mountains increases and the area of some inland lakes decreases, in turn leaving some influence on the results of the temperature.

The wind field does not vary as regularly as the temperature filed. Except for the variation of water body area which has a more consistent pattern on the wind field, all other types of underlying surface variation have a haphazard effect on the wind field (Fig. S4).
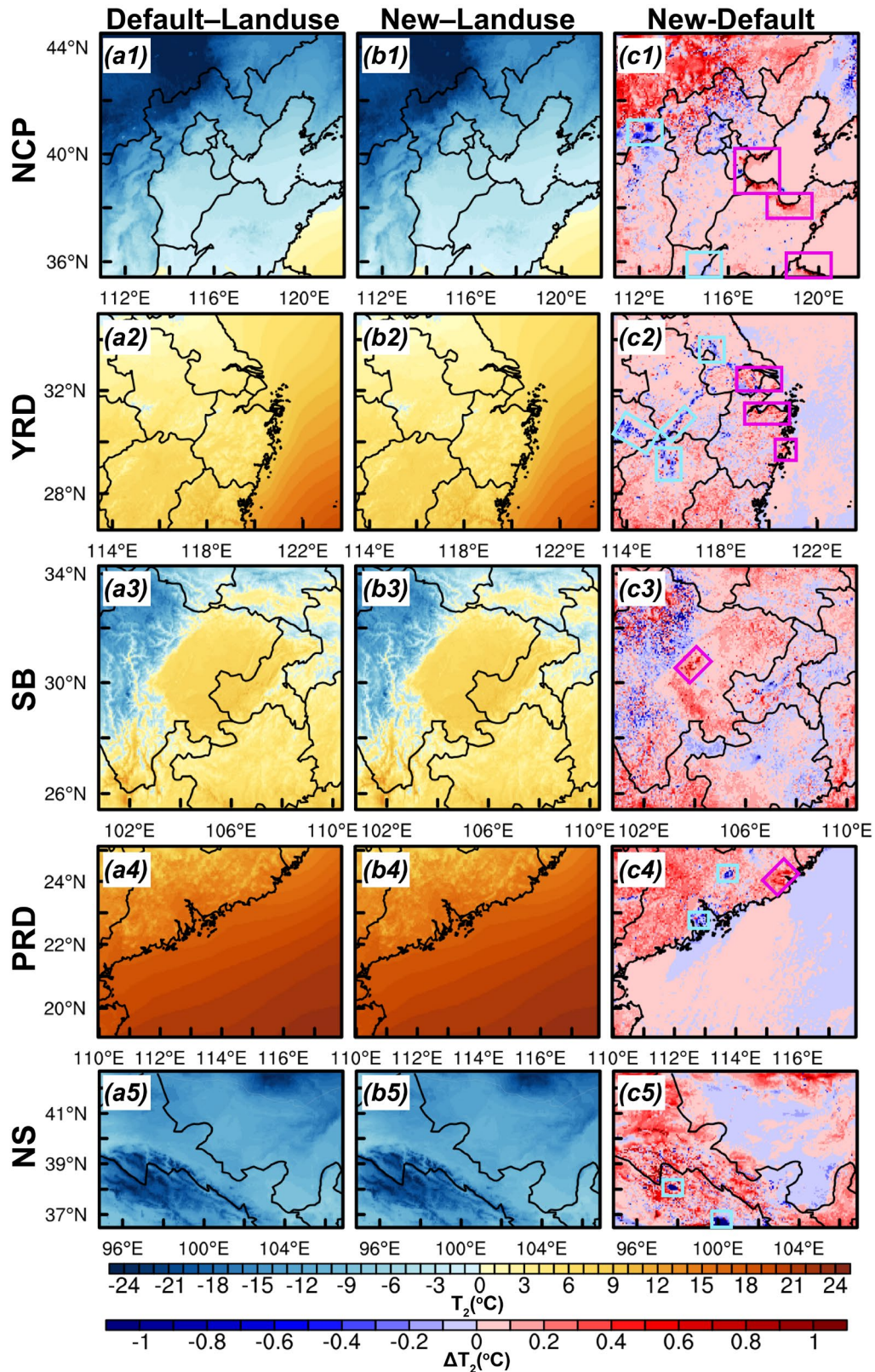
Figure 15. Regional distribution of 2-m temperature simulated by the (a) default land use, (b) new land use and (c) the difference between the two land use types for five regions in January. The blue (red) box indicates the region where the wind speed decreases (increases) due to changes in the water bodies and urban.

3.6 impact of the model version update

As computer technology continues to evolve, the parameterizations in the model are being upgraded and improved, but it is worthwhile further exploring how much the parameterizations and versions affect the simulation results of the model. For the PBL parameterization scheme, turbulent diffusion is crucial for the vertical mixing of momentum, heat, water vapor and pollutants within the PBL. And in December 2014, the ACM2 parameterization scheme received two major updates: (1) The turbulent diffusion coefficients of heat are updated. The stability function of Richardson number is modified, expecting to reduce the day and night 2-m temperature bias. (2) The bug that the minimum value of the PBLH is lower than the height of the first level of the model under stable conditions has been restored, and the minimum value of the PBLH is fixed to the height of the first level of the model. We, therefore, choose the ACM2 scheme in WRFv3.6.1 as a control experiment. In the control experiment, the ACM2 scheme in the WRFv3.9.1 version is replaced with WRFv3.6.1, and all other schemes are kept in the WRFv3.9.1 (i.e., WRFv3.6.1[+]). This ensures that the difference between the two experiments is the representative of the impact of the ACM2 scheme update.
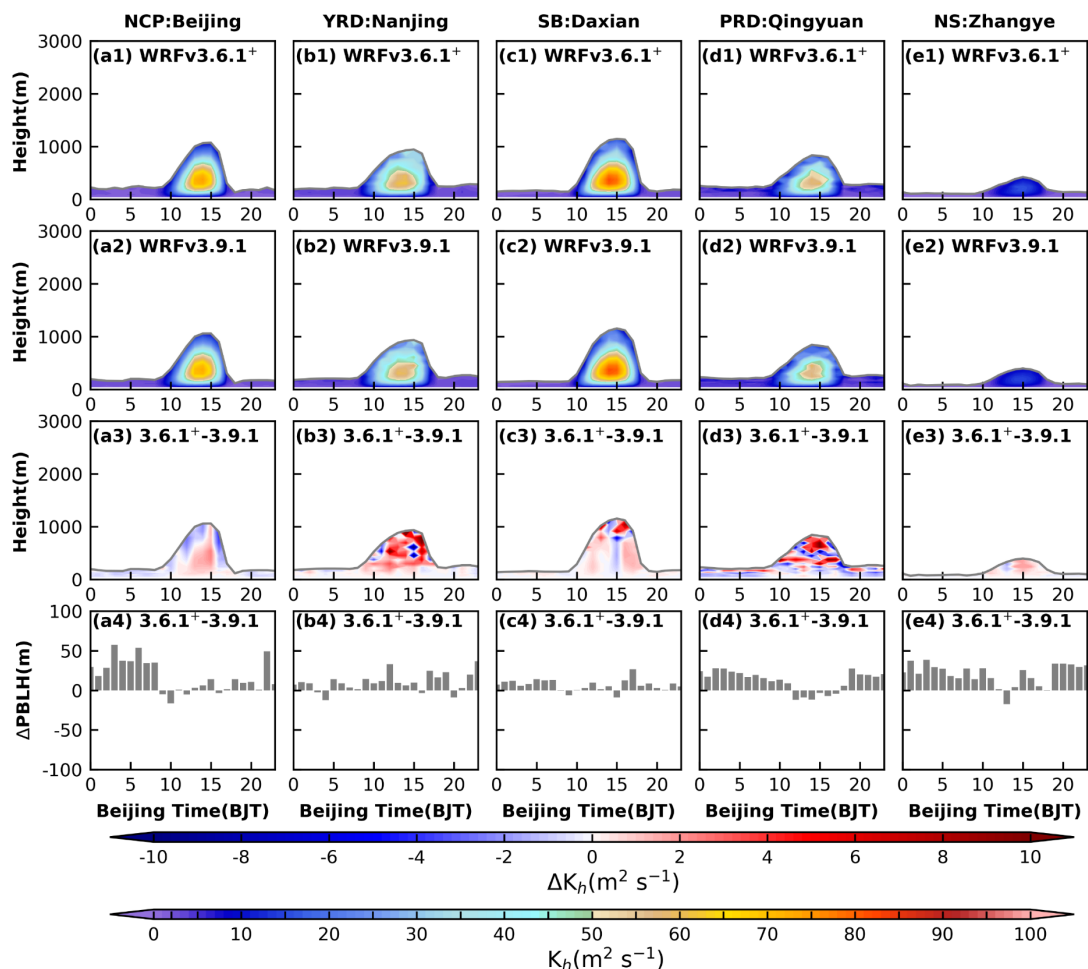
439   **Figure 16. Time-height cross sections of heat turbulent diffusion coefficient (TDC) simulated by**

440   **(a1-e1) WRFv3.6.1[+], (a2-e2) WRFv3.9.1, (a3-e3) the difference between the TDC of the two versions.**

441   **(a4-e4) Time series of diurnal variation of the difference between the PBLH of the two versions.**

442   **The gray line in (a1-e3) indicates the PBLH.**

443

444
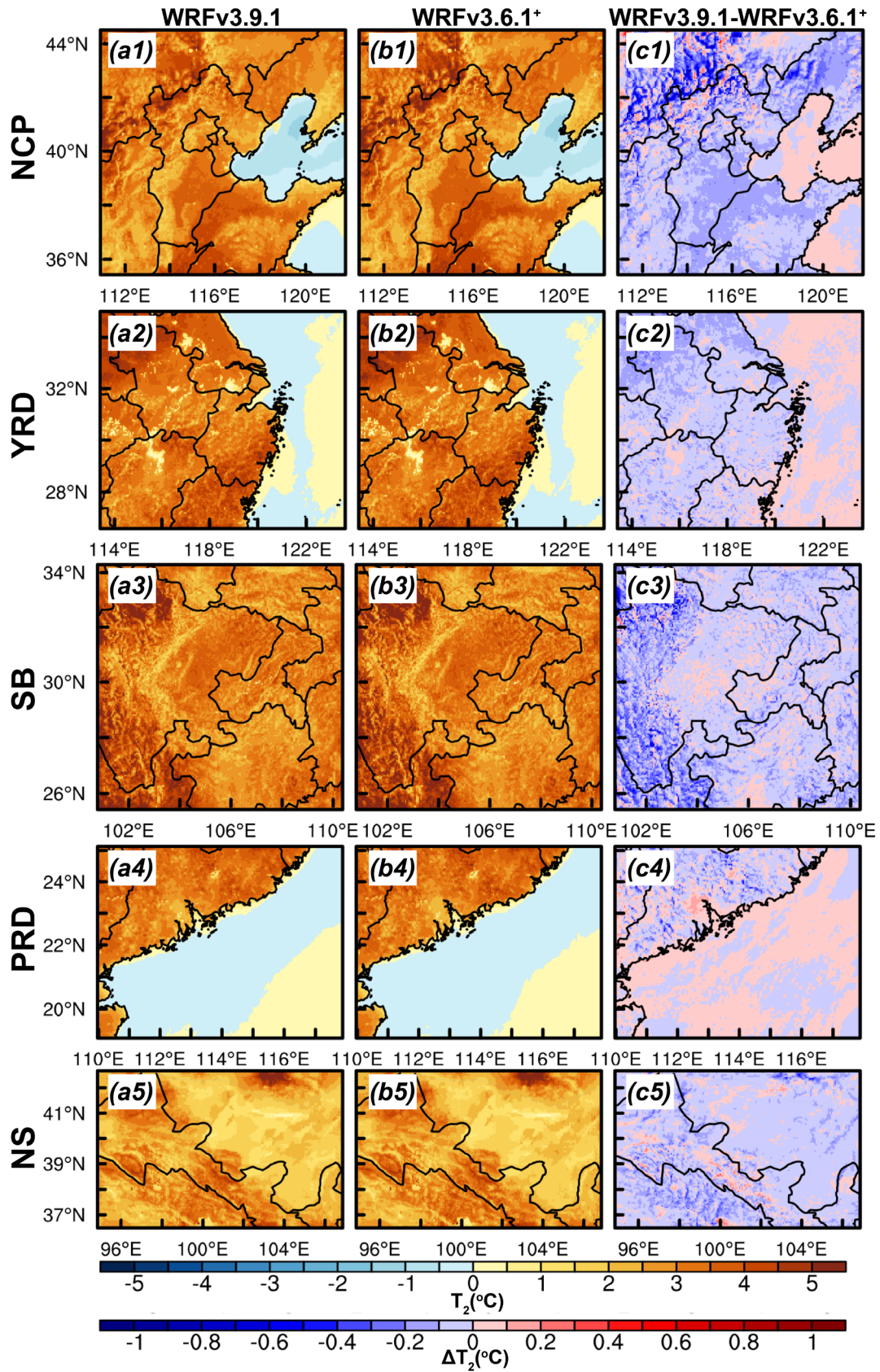
Figure 17. Regional distribution of diurnal 2-m temperature range simulated by the (a) WRFv3.9.1, (b) WRFv3.6.1⁺ and (c) the difference between the two versions for five regions in January.

447 The difference between the turbulent diffusion coefficient of heat calculated by the two versions lies

448 in the different principles of calculation using the Richardson number (Ri) method. In the

449 WRFv3.6.1[+], not only Ri is used to judge the stability, but also z/L is used to additionally constrain

450 the stability and determine the empirical stability function. In contrast, only Ri is adopted to

451 determine the function in the WRFv3.9.1. Figure 16 shows the diurnal variation of turbulent

452 diffusion coefficient of heat with height, as well as the difference of PBLH. In general, the two

453 versions have no effect on the overall trend of TDC (Fig. 16 a1-e2). However, within the PBL, the

454 TDC of WRFv3.9.1 is smaller than that of WRFv3.6.1[+], with the most significant difference during

455 the daytime. Meanwhile, in some regions at night, a TDC of WRFv3.9.1 is also greater than that of

456 WRFv3.6.1[+] (Fig. 16 a3-e3). Besides, the differences among the five regions slightly vary. The

457 deviation in the NCP, SB, and NS regions is small, around 2 m^2 s^{-1} (Fig. 16 a3, c3, e3), while the

458 deviation in the YRD and PRD regions is large, up to about 10 m^2 s^{-1} (Fig. 16 b3, d3). The TDC

459 modification aims to reduce the temperature difference between day and night. Indeed, this

460 expectation is fulfilled. It can be noticed in figure 17, the diurnal temperature difference for

461 WRFv3.9.1 is smaller than that of WRFv3.6.1[+] in almost all regions (except for the area where the

462 underlying surface is water). In addition, we need to pay attention to the variation of the PBLH. As

463 shown in figure 16, the difference in PBLH during daytime is smaller than at night, and the PBLH

464 of WRFv3.9.1 is lower than that of WRFv3.6.1[+]. The model WRFv3.9.1 fixes the minimum value

465 of the PBLH to the first level height, markedly reducing the PBLH at night. But this approach may

466 be too crude and parsimonious to cause problems, and should be corrected in the future.

4 Conclusion

468 The simulation results of the model within the PBL are subject to many factors, but its portrayal and

469 description by the PBL parameterization schemes plays a vital role in affecting the variation of the

470 meteorological field. The simulations of the PBL schemes on the meteorological fields has been

471 described in Part I. In Part II, further uncertainties affecting the results of the meteorological field

472 are evaluated and analyzed, and the degree of influence of different factors is compared, hoping to

473 provide a reference for scholars conducting research on the model.

474 In addition to the dominant role of the PBL scheme on the results of the meteorological field, many

475 elements in the model are influenced by large uncertainties. For example, what is the effect of

476 horizontal resolution, and how much does the result vary under different resolution conditions? Is

477   the continuous encryption of the vertical levels necessary for the simulation of the vertical structure

478   of the PBL? Which has a greater impact on the results of the meteorological field, the near-surface

479   (N-S) layer scheme or the PBL scheme? How much is the impact of these changes on the underlying

480   surface, which is constantly updated by the development of urbanization? The innovation of

481   computer technology has brought the opportunity to keep the model being updated. How much

482   effect will the updates have on different versions of the model results? The simulation of the model

483   depends on the initial and boundary conditions, so how much does the initial and boundary

484   conditions of different resolutions and products affect the model results? These uncertainties have

485   not been fully evaluated and analyzed yet. To resolve the confusions, this study synthesizes the

486   effects of the above factors on the model results.
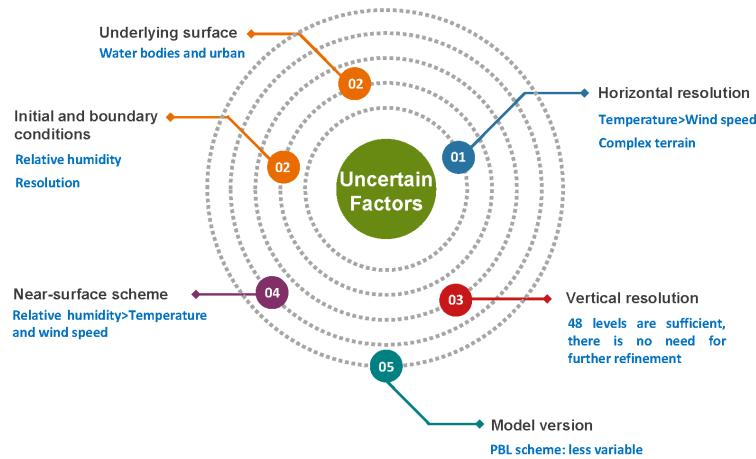
487
488   **Figure 18. An overview figure of the prioritization of uncertainties, where the uncertainties are in**
489   **black font and the elements focused on in that factor are in blue font.**

490   *a. Effect of the horizontal resolution.* The three different resolutions have a more dramatic effect

491   on temperature than on wind speed (Fig. 18). Regardless of the region, the distribution of

492   temperature deviations simulated at 75 km resolution is clearly different from that of 15 km and

493   3 km, especially in areas with more complex topography, such as NCP, SB and NS regions. All

494   three resolutions overestimate the wind speed in all regions, except for the 75 km resolution,

495   where there is an underestimation of the wind speed at the stations around the basin in the SB

496   region (Fig. 18). The difference between the resolutions decreases with increasing temperature,

497   but becomes more pronounced with increasing wind speed.

498   *b. Effect of the vertical resolution.* The number of vertical levels of the model is encrypted from

499   48 to 62 levels, with almost no effect on the vertical structure of the PBL. Meanwhile, the

500   increase in the number of vertical levels brings into an increase in memory of about 150 GB for

501   one month. Compared to the horizontal resolution, the vertical resolution does not need to be

| 502 | set particularly fine, and 48 levels are perfectly sufficient to reproduce the evolution of the PBL |
| 503 | structure (Fig. 18). |

504   *c.*   ***Influence of the N-S scheme.*** The PBL scheme makes a greater impact on the simulated results
505   for temperature, wind speed and direction, while for relative humidity, the N-S scheme
506   contributes largely, especially in the NCP, SB and NS regions. For either scheme, the effect is
507   much greater at night than during the daytime. In general, the choice of the PBL scheme is more
508   critical for temperature and wind fields. But for relative humidity, the PBL and N-S schemes
509   are equally important (Fig. 18).

510   *d.*   ***Impact of the initial and boundary conditions.*** The effect of data of different resolutions of the
511   same product on the results of temperature and relative humidity is small, but the influence of
512   data of different products of the same resolution is large. EC data simulates temperature better
513   than FNL data during the daytime, while at night, the difference between the two data is
514   relatively small (except for the NCP and NS regions). The EC data simulate the relative
515   humidity better than the FNL data regardless of the region, even in the vertical direction, which
516   will expose a key way to improve the relative humidity results of the model in the future (Fig.
517   18). Nonetheless, data of the same resolution but different products exhibit no obvious effect
518   on wind speed, while the influence of data from the same product with different resolutions is
519   larger, especially at night.

520   *e.*   ***Effect of the underlying surface.*** In terms of regional distribution, the new underlying surface
521   make no significant difference with respect to the temperature. However, for the grids with
522   more pronounced changes in water bodies and urban, the change in underlying surface has an
523   approximate ±1°C influence on temperature (Fig. 18). An increase (decrease) in the area of
524   water bodies leads to an increase (decrease) in temperature, and the growth of urbanization
525   brings about an increase in temperature. The variation of wind field is not as regular as
526   temperature. Except for the changes in the area of water bodies that affect the wind filed
527   consistently, other types of underlying surface changes show a haphazard effect on the wind
528   filed.

529   *f.*   ***Influence of the model version.*** The update of the PBL scheme reduces the day and night 2-m
530   temperature bias. But the simple definition method of fixing the minimum value of the PBLH
531   as the first level height of the model may have some defects. The change in the stability function
532   of the Richardson number alters the turbulent diffusion coefficient of heat, which is more

533 distinct in the daytime with a deviation of about 10 m^2 s^{-1}. The PBL parameterization scheme

534 in the current model is less modified (Fig. 18).

535 In summary, the horizontal resolution is more influential than the vertical resolution. The N-S

536 scheme has less effect than the PBL scheme on the results of temperature and wind speed. Also,

537 the initial and boundary conditions of different products have the most significant influence on

538 relative humidity. Grid changes where the underlying surface is urban and water bodies have a

539 more pronounced effect on the results of meteorological fields, especially for temperature. The

540 PBL parameterization schemes in the version WRFv3.9.1 and WRFv3.6.1 are less changed and

541 have less impact on the simulation of model results. (Fig. 18). A special advice here is that the

542 needs of different scholars for the model vary a lot, thus, the configuration of uncertainties

543 requires a comprehensive consideration to obtain the optimal results for the analysis.

544 **Code and data availability**

545 The source codes of WRF version 3.9.1 and 3.6.1 can be found on the following website:

546 https://www2.mmm.ucar.edu/wrf/users/download/. The original model settings file is already

547 included in Supplement in Part I, while the other model settings file used in Part II is named after

548 the file name "L62_namelist.input" and is already included in Supplement. In addition, the

549 observations used are also provided in Supplement in Part I. The initial field and boundary condition

550 data and the underlying surface data are provided in the text.

551 **Author contributions**

552 Development of the ideas and concepts behind this work was performed by all the authors. Model

553 execution, data analysis and paper preparation were performed by WJ. XZ and HW provide

554 computing resources, and offer advice and feedback. YW, DW, and JZ support the data. WZ, LZ,

555 LG, YL, JW, YY, and YL provides suggestions. All authors contributed to the manuscript.

556 **Competing interests**

557 The authors declare that they have no conflict of interest.

558 **Acknowledgements.**

559 The work was carried out at the National Supercomputer Center in Tianjin, and the calculations

560 were performed on TianHe-1 (A).

Financial support

This research is supported by NSFC Major Project (42090031), NSFC Project (U19A2044), Basic Research Fund of CAMS (2023Y003).

References

Bhati, S., andMohan, M. WRF model evaluation for the urban heat island assessment under varying land use/land cover and reference site conditions. *Theoretical and Applied Climatology, 126*(1), 385-400. doi:10.1007/s00704-015-1589-5. 2016

Chang, P., Zhang, S., Danabasoglu, G., Yeager, S. G., Fu, H., Wang, H., et al. An Unprecedented Set of High-Resolution Earth System Simulations for Understanding Multiscale Interactions in Climate Variability and Change. *Journal of Advances in Modeling Earth Systems, 12*(12), e2020MS002298. doi:10.1029/2020MS002298. 2020

Friedl, M. A., McIver, D. K., Hodges, J. C. F., Zhang, X. Y., Muchoney, D., Strahler, A. H., et al. Global land cover mapping from MODIS: algorithms and early results. *Remote Sensing of Environment, 83*(1), 287-302. doi:10.1016/S0034-4257(02)00078-0. 2002

García-García, A., Cuesta-Valero, F. J., Beltrami, H., González-Rouco, J. F., andGarcía-Bustamante, E. WRF v.3.9 sensitivity to land surface model and horizontal resolution changes over North America. *Geosci. Model Dev., 15*(2), 413-428. doi:10.5194/gmd-15-413-2022. 2022

Jia, W., andZhang, X. The role of the planetary boundary layer parameterization schemes on the meteorological and aerosol pollution simulations: A review. *Atmospheric Research, 239*. doi:10.1016/j.atmosres.2020.104890. 2020

Li, D., Chang, P., Yeager, S. G., Danabasoglu, G., Castruccio, F. S., Small, J., et al. The Impact of Horizontal Resolution on Projected Sea-Level Rise Along US East Continental Shelf With the Community Earth System Model. *J Adv Model Earth Syst, 14*(5), e2021MS002868. doi:10.1029/2021MS002868. 2022

Li, J., Bao, Q., Liu, Y., Wang, L., Yang, J., Wu, G., et al. Effect of horizontal resolution on the simulation of tropical cyclones in the Chinese Academy of Sciences FGOALS-f3 climate system model. *Geosci. Model Dev., 14*(10), 6113-6133. doi:10.5194/gmd-14-6113-2021. 2021

Li, Y., Gao, Z., Lenschow, D. H., andChen, F. An Improved Approach for Parameterizing Surface-Layer Turbulent Transfer Coefficients in Numerical Models. *Boundary-Layer Meteorology, 137*(1), 153-165. doi:10.1007/s10546-010-9523-y. 2010

Ma, Z., Liu, Q., Zhao, C., Shen, X., Wang, Y., Jiang, J. H., et al. Application and Evaluation of an Explicit Prognostic Cloud-Cover Scheme in GRAPES Global Forecast System. *Journal of*

Advances in Modeling Earth Systems, 10(3), 652-667. doi:10.1002/2017MS001234. 2018

Ma, Z., Zhao, C., Gong, J., Zhang, J., Li, Z., Sun, J., et al. Spin-up characteristics with three types of initial fields and the restart effects on forecast accuracy in the GRAPES global forecast system. *Geoscientific Model Development, 14*(1), 205-221. doi:10.5194/gmd-14-205-2021. 2021

Magnusson, L., andKällén, E. Factors Influencing Skill Improvements in the ECMWF Forecasting System. *Monthly Weather Review, 141*(9), 3142-3153. doi:10.1175/mwr-d-12-00318.1. 2013

Menut, L., Bessagnet, B., Colette, A., andKhvorostiyanov, D. On the impact of the vertical resolution on chemistry-transport modelling. *Atmospheric Environment, 67*, 370-384. doi:10.1016/j.atmosenv.2012.11.026. 2013

Morichetti, M., Madronich, S., Passerini, G., Rizza, U., Mancinelli, E., Virgili, S., et al. Comparison and evaluation of updates to WRF-Chem (v3.9) biogenic emissions using MEGAN. *Geosci. Model Dev., 15*(16), 6311-6339. doi:10.5194/gmd-15-6311-2022. 2022

Nolan, D. S., andOnderlinde, M. J. The Representation of Spiral Gravity Waves in a Mesoscale Model With Increasing Horizontal and Vertical Resolution. *Journal of Advances in Modeling Earth Systems, 14*(8), e2022MS002989. doi:10.1029/2022MS002989. 2022

O'Dea, E., Furner, R., Wakelin, S., Siddorn, J., While, J., Sykes, P., et al. The CO5 configuration of the 7 km Atlantic Margin Model: large-scale biases and sensitivity to forcing, physics options and vertical resolution. *Geosci. Model Dev., 10*(8), 2947-2969. doi:10.5194/gmd-10-2947-2017. 2017

Ouyang, Z., Sciusco, P., Jiao, T., Feron, S., Lei, C., Li, F., et al. Albedo changes caused by future urbanization contribute to global warming. *Nature Communications, 13*(1), 3800. doi:10.1038/s41467-022-31558-z. 2022

Qian, Y., Chakraborty, T. C., Li, J., Li, D., He, C., Sarangi, C., et al. Urbanization Impact on Regional Climate and Extreme Weather: Current Understanding, Uncertainties, and Future Research Directions. *Adv Atmos Sci, 39*(6), 819-860. doi:10.1007/s00376-021-1371-9. 2022

Roberts, M. J., Jackson, L. C., Roberts, C. D., Meccia, V., Docquier, D., Koenigk, T., et al. Sensitivity of the Atlantic Meridional Overturning Circulation to Model Resolution in CMIP6 HighResMIP Simulations and Implications for Future Changes. *Journal of Advances in Modeling Earth Systems, 12*(8), e2019MS002014. doi:10.1029/2019MS002014. 2020

Rummukainen, M. Added value in regional climate modeling. *WIREs Climate Change, 7*(1), 145-159. doi:10.1002/wcc.378. 2016

Schwaab, J., Meier, R., Mussetti, G., Seneviratne, S., Bürgi, C., andDavin, E. L. The role of urban trees in reducing land surface temperatures in European cities. *Nature Communications,*

631   *12*(1), 6763. doi:10.1038/s41467-021-26768-w. 2021

632   Singh, J., Singh, N., Ojha, N., Sharma, A., Pozzer, A., Kiran Kumar, N., et al. Effects of spatial

633   resolution on WRF v3.8.1 simulated meteorology over the central Himalaya. *Geosci. Model*

634   *Dev., 14*(3), 1427-1443. doi:10.5194/gmd-14-1427-2021. 2021

635   Small, R. J., Bacmeister, J., Bailey, D., Baker, A., Bishop, S., Bryan, F., et al. A new synoptic scale

636   resolving global climate simulation using the Community Earth System Model. *Journal of*

637   *Advances in Modeling Earth Systems, 6*(4), 1065-1094. doi:10.1002/2014MS000363. 2014

638   Taylor, K. E., Stouffer, R. J., andMeehl, G. A. An Overview of CMIP5 and the Experiment Design.

639   *Bulletin of the American Meteorological Society, 93*(4), 485-498. doi:10.1175/bams-d-11-

640   00094.1. 2012

641   Teixeira, J. C., Carvalho, A. C., Tuccella, P., Curci, G., andRocha, A. WRF-chem sensitivity to

642   vertical resolution during a saharan dust event. *Physics and Chemistry of the Earth, Parts*

643   *A/B/C, 94*, 188-195. doi:10.1016/j.pce.2015.04.002. 2016

644   Tolentino, J., Rejuso, M. V., Inocencio, L. C., Ang, M. R. C., andBagtasa, G. (2016). *Effect of*

645   *horizontal and vertical resolution for wind resource assessment in Metro Manila, Philippines*

646   *using Weather Research and Forecasting (WRF) model* (Vol. 10005): SPIE.

647   Wang, L., andLi, D. Urban Heat Islands during Heat Waves: A Comparative Study between Boston

648   and Phoenix. *Journal of Applied Meteorology and Climatology, 60*(5), 621-641.

649   doi:https://doi.org/10.1175/JAMC-D-20-0132.1. 2021

650   Weigel, A. P., Chow, F. K., andRotach, M. W. The effect of mountainous topography on moisture

651   exchange between the "surface" and the free atmosphere. *Boundary-Layer Meteorology,*

652   *125*(2), 227-244. doi:10.1007/s10546-006-9120-2. 2007

653   Zhou, B., Zhu, K., andXue, M. A Physically Based Horizontal Subgrid-Scale Turbulent Mixing

654   Parameterization for the Convective Boundary Layer. *Journal of the Atmospheric Sciences,*

655   *74*(8), 2657-2674. doi:10.1175/jas-d-16-0324.1. 2017

656